How well do we characterize snow storage in High Mountain Asia?

Yufei Liu[1], Yiwen Fang[1], Dongyue Li[2], and Steven A Margulis[2]

[1]University of California, Los Angeles
[2]University of California Los Angeles

November 23, 2022

Abstract

Accurate characterization of peak snow water storage in High Mountain Asia (HMA) is essential for assessing the water supply to over one billion downstream residents. Currently, such characterization still relies on modeling due to the measurement scarcity. Here, eight global snow products were examined over HMA using a newly developed High Mountain Asia Snow Reanalysis (HMASR) dataset as a reference. The focus of intercomparison was on peak annual snow storage, the first-order determinant of warm-season water availability in snow-dominated basins. Across eight products the climatological peak storage over HMA was found to be 161 $km^3 \pm 102$ km^3 with an average 33% underestimation relative to HMASR. The inter-product variability in cumulative snowfall (335 $km^3 \pm 148$ km^3) explains the majority (>80%) of peak snow storage uncertainty, while significant snowfall loss to ablation during accumulation season (51% ± 9%) also reveals the critical role of ablation processes on peak snow storage.

How well do we characterize snow storage in High Mountain Asia?

Yufei Liu[1], Yiwen Fang[1], Dongyue Li[1] and Steven A. Margulis[1]

[1] Department of Civil and Environmental Engineering, University of California, Los Angeles, Los Angeles, CA, 90095.

Corresponding author: Steven A. Margulis (margulis@seas.ucla.edu)

Key Points:

- Existing snow products generally underestimate peak snow storage in High Mountain Asia compared with a novel snow reanalysis dataset
- Large inter-product variability in accumulation-season snowfall explains most of the uncertainty in peak snow storage
- Accumulation-season ablation plays a significant role in peak snow storage uncertainty and deserves more attention in future studies

Abstract

Accurate characterization of peak snow water storage in High Mountain Asia (HMA) is essential for assessing the water supply to over one billion downstream residents. Currently, such characterization still relies on modeling due to the measurement scarcity. Here, eight global snow products were examined over HMA using a newly developed High Mountain Asia Snow Reanalysis (HMASR) dataset as a reference. The focus of intercomparison was on peak annual snow storage, the first-order determinant of warm-season water availability in snow-dominated basins. Across eight products the climatological peak storage over HMA was found to be 161 km^3 $\pm$ 102 km^3 with an average 33% underestimation relative to HMASR. The inter-product variability in cumulative snowfall (335 $km^3 \pm$ 148 km^3) explains the majority (>80%) of peak snow storage uncertainty, while significant snowfall loss to ablation during accumulation season (51% $\pm$ 9%) also reveals the critical role of ablation processes on peak snow storage.

Plain Language Summary

Peak snow storage is important for summer and fall water availability in snow-dominated regions. Here, we evaluated the estimates of peak snow storage over High Mountain Asia (HMA) from eight global snow products with respect to the newly developed High Mountain Asia Snow Reanalysis (HMASR). The results suggest a large uncertainty and general underestimation (33%) in HMA-wide peak snow storage estimates across the global snow products, when compared to the reference HMASR. Inter-product snowfall variability among global snow products explains most of their peak snow storage uncertainty (over 80%). Significant snow ablation loss during the accumulation season (~50% of snowfall inputs) is also critical in contributing to the peak snow storage variations.

1 Introduction

Seasonal snow accumulation in global mountain “water towers” provides a virtual reservoir in winter that is essential for warm-season water supply (Viviroli et al., 2007). In High Mountain Asia (HMA), snowmelt feeds the major river basins (e.g. Indus, Amu Darya, Ganges) in their headwaters (Bookhagen and Burbank, 2010; Armstrong et al., 2019; Khanal et al., 2021; Kraaijenbrink et al., 2021), which is critical for meeting the human water demands of over 1 billion people in spring and summer (Immerzeel et al., 2010). Snow storage in seasonal snowpacks and the timing of snowmelt are highly sensitive to a warming climate, which is likely to alter the frequency of snow droughts (Huning and AghaKouchak, 2020) and pose risks to the water security for natural and human use (Immerzeel et al., 2020; Qin et al., 2020; Kraaijenbrink et al., 2021).

Snow water equivalent (SWE) is directly indicative of the total water resource availability in snowpacks at a given time. SWE reaches its seasonal peak at the end of the accumulation season (right before melt onset); accurately estimating peak snow storage (and its spatial distribution) is thus a first-order requirement for assessing snow-derived water availability for downstream use (Li et al., 2019). Despite its importance, the quantification of peak SWE over the world’s mountains is still poorly constrained (Mudryk et al., 2015; Wrzesien et al., 2019), primarily due to the difficulties in directly measuring SWE, which is impeded by the scarcity or the non-existence of in situ gages in many critical regions and a lack of satellite-based remote sensing for globally consistent SWE measurements (Palazzi et al., 2013; Dozier et al., 2016; Bormann et al., 2018). SWE can be estimated through data assimilation and modeling approaches. However, previous intercomparison studies suggest large discrepancies in SWE estimation over the entire northern hemisphere (Mudryk et al., 2015; Mortimer et al., 2020; Xiao et al., 2020), North America or the Western United States (WUS; McCrary and Mearns, 2019; Wrzesien et al., 2019; Xu et al., 2019; Kim et al., 2021; Cho et al., 2022), Hindu Kush-Karakoram-Himalaya (Terzago et al., 2014), and the Tibetan Plateau (Bian et al., 2019; Orsolini et al., 2019). Despite the large uncertainties seen across the SWE products, studies assessing the links between snowpack storage, water availability and climate change are often based on a single snow dataset (e.g. Mankin et al., 2015; Huning and AghaKouchak, 2020; Immerzeel et al., 2020; Qin et al., 2020), which propagates the error in snow storage estimates to climatic and water resource availability quantification. Without improved characterization of seasonal snow storage, in regions like HMA, where the downstream regions have the densest population on Earth (over one billion residents in total) and the water supply to these residents heavily relies on snow-derived water, our confidence in estimating water resource availability and how it has been changing will remain compromised, thus impacting our ability to effectively adapt to ongoing changes.

In this study, the newly developed High Mountain Asia Snow Reanalysis (HMASR; Liu et al., 2021a, b) is employed as a reference SWE dataset to examine the peak snow storage estimates from eight global atmospheric reanalysis and land data assimilation products. The use of HMASR provides a new reference dataset, derived specifically for mountain domains and constrained by remote sensing observations, to perform a more thorough evaluation of snow storage estimates over the broad HMA domain. The focus herein is understanding the uncertainty in processes leading up to accumulation-season peak SWE storage due to its first-order determination of available water resources in snow-dominated regions. The novelty of this study is embedded in the answers to the following science questions:

1. What is the uncertainty in peak snow water storage over High Mountain Asia and its watersheds?

2. How much of the uncertainty in peak snow storage is explained by the variability in accumulation-season snowfall and ablation, respectively?

2 Data

Herein the reference SWE dataset (HMASR) and eight reanalysis datasets are examined. The eight global datasets (Text S1 and Table S1) are chosen as representative community-based global products that span most of the period of HMASR (1999-2017), including: ERA5 and ERA5-land (European Centre for Medium-Range Weather Forecasts (ECMWF) Re-Analysis products, 5th generation; Hersbach et al., 2020; Muñoz-Sabater et al., 2021), MERRA2 (Modern-Era Retrospective analysis for Research and Applications, version 2; Gelaro et al., 2017), JRA55 (Japanese 55-year Reanalysis; Kobayashi et al., 2015) and four GLDAS-2.1 products (Global Land Data Assimilation System version 2.1; Rodell et al., 2004) at several resolutions and with different land surface models (GLDAS-Noah (0.25°), GLDAS-Noah (1°), GLDAS-VIC (1°), and GLDAS-CLSM (1°), details listed in Table S1). Hereafter, to distinguish the globally-available datasets and the reference dataset, we use “snow products” and “HMASR” respectively.

The intercomparison study period is chosen as Water Years (WYs) 2001 to 2017, with the maximum overlap across all datasets (Table S1; with WY 2001 spanning from 1 October 2000 to 30 September 2001 for example). All nine datasets provide SWE estimates to evaluate the peak seasonal water storage. Other meteorological forcings (precipitation, P; air temperature, T_a; and snowfall, S) are obtained from the global snow products. HMASR (which does not include snowfall) provides only SWE for comparison. The meteorological forcing variables for each snow product are obtained at their raw spatial and temporal resolutions (Table S1) and are aggregated into daily total values (for P and S) or daily average values (for T_a). Spatial aggregation is also performed for SWE and meteorological forcings to facilitate the intercomparison and the analysis at the basin- or domain-scale (Sections 4.1).

3 Study region and Methods

3.1 Study domain and classification of seasonal, ephemeral, and persistent snow regions

The HMA region (Figure 1a) includes key mountain ranges (e.g. Tien Shan, Pamir, Karakoram, Himalayas, etc.) and the Tibetan Plateau. Westerlies dominate winter precipitation in the northwest and the Indian and East Asia monsoons dominate summer precipitation in the southeast (Yao et al., 2012).

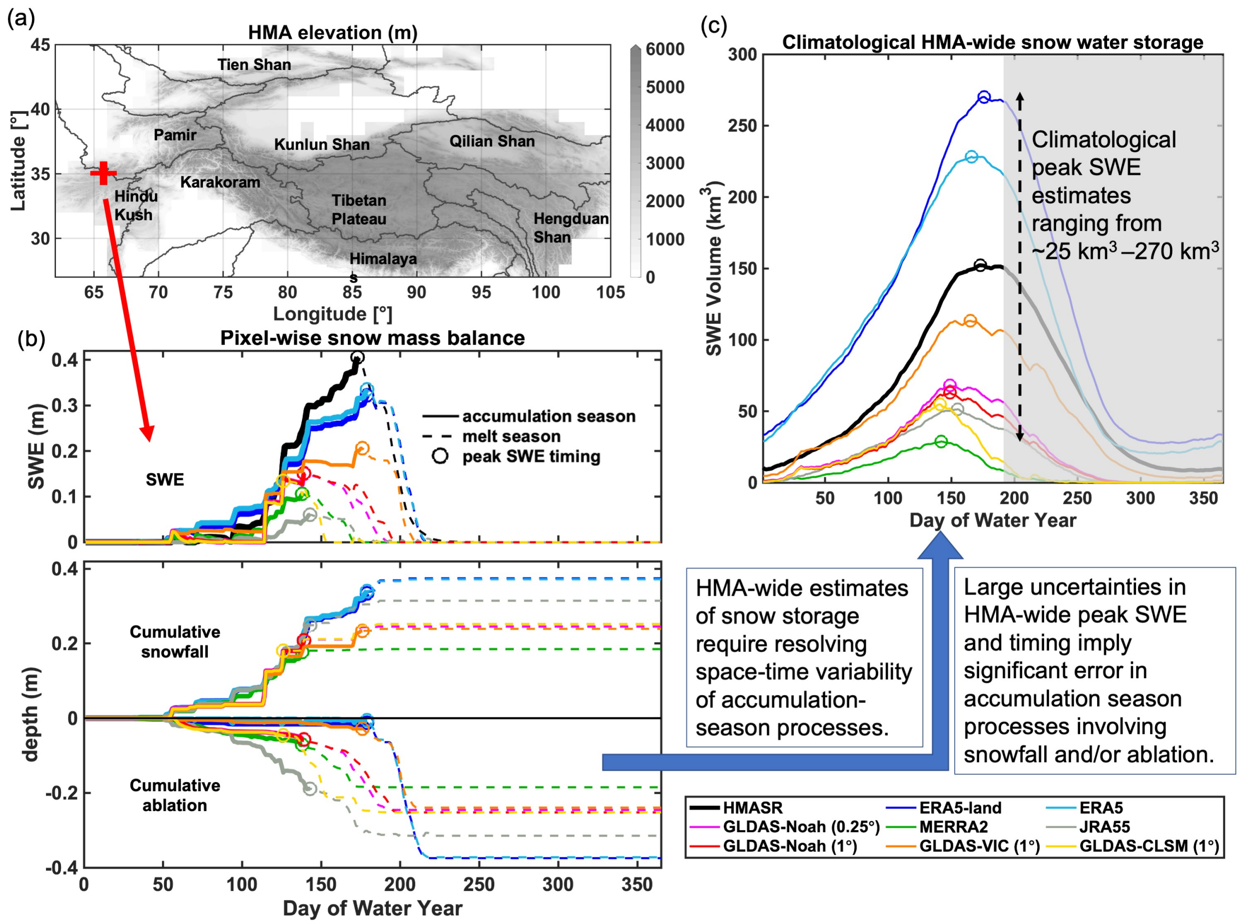

Figure 1. **a**) map of HMASR domain elevation with major watershed boundaries. The red '+' symbol indicates the location shown in (b); **b**) an illustrative example of the seasonal cycle of SWE, cumulative snowfall, and cumulative ablation at a representative pixel in WY2017. The solid curves represent processes leading up to peak SWE (the focus of the work described herein), and the dashed curves represent the processes after peak SWE. The 'o' symbols on the curves

indicate peak SWE timing; **c**) the 17-year climatology of the seasonal cycle of HMA-wide SWE volume. The colors of the curves in (**b**) and (**c**) represent the estimation from different datasets.

3.2 Accumulation-season snow mass balance

Snowpack evolution can be characterized as snow mass gain (via solid precipitation, i.e. snowfall) and snow mass loss (via ablation, e.g. snowmelt, sublimation, wind drifting, etc.), which can be represented with mass and energy balance (Liston and Elder, 2006; McCrary and Mearns, 2019). Herein we only focus on accumulation-season processes, as accurately characterizing peak storage is a necessary condition for accurately representing ablation-season processes and the total snowmelt water resource availability.

We start with defining the snow accumulation season at the pixel-scale (from day of water year (DOWY) 1 until pixel-wise peak SWE DOWY, Text S2 and Figure S1). Note that 'accumulation season' is most robustly defined for seasonal snow rather than ephemeral snow, as the latter is intermittent, where snow may accumulate and fully disappear multiple times within a WY (Petersky and Harpold, 2018). Both seasonal and ephemeral snow are important types (Sturm et al. 1995), while the former is more critical for water supply and thus emphasized in this work. Through the snow mass balance within the accumulation season (Text S3), we obtain the relationship:

$$swe_{peak} = s_{acc} - a_{acc} \tag{1}$$

where swe_{peak} is the pixel-wise peak SWE, and s_{acc} and a_{acc} respectively denote the cumulative snowfall and snow ablation integrated over the accumulation season.

In this work, both swe_{peak} and s_{acc} are obtained from the snow products, and a_{acc} is computed as the difference between s_{acc} and swe_{peak} (Text S3). Figure 1b provides an illustrative example showing the seasonal cycle of SWE, cumulative snowfall and ablation at a representative pixel in WY2017, showing clear differences in swe_{peak} and its timing across products. Note that this comparison is primarily for illustration due to the large grid size differences among datasets. We also provide the caveat in using JRA55 that the diagnosed a_{acc} is likely a mix of model-specific ablation processes and non-negligible data assimilation corrections (Text S3).

The focus of this study is to quantitatively compare the seasonal snow storage estimates over the full HMA domain and at subregional scales through integrating pixel-scale quantities into basin- or HMA-scale volumes. Herein the 10 largest watersheds in HMA are examined (Lehner et al., 2008) and shown in Figure 1a. Seasonal, ephemeral, and persistent snow masks (Figure S2; Table S2; Text S4) are applied prior to the integration, with persistent snow excluded in the volume integration. For the three quantities in equation (1), the spatially integrated volumes are denoted herein as SWE_{peak}, S_{acc} and A_{acc} (in units of km^3), with the same relationship:

$$SWE_{peak} = S_{acc} - A_{acc} \tag{2}$$

It should be noted that A_{acc} is calculated as the difference between S_{acc} and SWE_{peak} as noted earlier. Spatial integration over elevation bands (using intervals of 1000 m) is also performed in this work (Text S5; Figure S3).

The analysis presented in this work consists of examining SWE_{peak} across all datasets (including using HMASR as a reference) and additionally S_{acc} and A_{acc} across all snow products.

More specifically, a linear regression (Text S6) is applied to examine the variations in S_{acc} loss to A_{acc} and their ability to explain SWE_{peak} variance:

$$SWE_{peak} = \beta * S_{acc} + \varepsilon \quad (3)$$

where β is the regression coefficient (slope), and ε is the random noise. SWE_{peak} and S_{acc} are obtained from each product and for each WY. Note that JRA55 and HMASR data were excluded in the linear regression, since their snowfall data is either not available (HMASR) or inconsistent with SWE (JRA55, due to significant data assimilation corrections in SWE; Text S3).

4 Results and Discussion

4.1 Uncertainty in peak snow storage over HMA and its watersheds

4.1.1 HMA-scale

The integrated SWE volume climatology (17-year average) time series over HMA (Figure 1c) shows significant variations in peak storage (a range of ~240 km^3) and peak timing (a range of ~35 days). Among these snow products, the largest peak snow storage is an order of magnitude greater than the lowest storage, and the earliest peak timing is one month ahead of the latest, suggesting large uncertainty across snow products. To better understand what drives the HMA-wide storage differences and isolate accumulation-season sources of uncertainty, all results to follow focus on the pixel-wise peak snow storage (SWE_{peak}) and the processes leading to that storage (S_{acc} and A_{acc}).

The climatological HMA-wide SWE_{peak}(pixel-wise peak snow storage) estimate is 161 km^3 $\pm$ 102 km^3 across all global snow products (with HMASR as a standalone dataset for evaluation; Text S7 and Table S3), exhibiting a 63% uncertainty relative to the mean. When partitioned into seasonal and ephemeral snow, the estimates are 110 km^3 $\pm$ 74 km^3 and 51 km^3 $\pm$ 28 km^3, respectively. The ERA5-land and ERA5 snow products, with volumes of 341 km^3 and 288 km^3, exhibit larger values than HMASR (239 km^3), corresponding to 43% and 20% more snow respectively. The GLDAS estimates all exhibit less snow than HMASR, with estimates of GLDAS-VIC (179 km^3), GLDAS-Noah (120 km^3 and 114 km^3 for 0.25° and 1° respectively), and GLDAS-CLSM (98 km^3), corresponding to 25%, 50%, 53% and 59% less snow than HMASR. The JRA55 and MERRA2 products exhibit the lowest SWE_{peak} with 93 km^3 (61% less than HMASR) and 54 km^3 (77% less than HMASR), respectively. When the snow products are compared collectively to HMASR over the full HMA domain, the mean difference (MD) in SWE_{peak} is -33% with a root mean square difference (RMSD) of 52%. In seasonal snow regimes, there is a MD of -47% and RMSD of 58%. In ephemeral snow regimes, there is a MD of 70% and RMSD of 113%. This highlights the qualitative differences across snow regimes (underestimation in seasonal vs. overestimation in ephemeral) that are partially canceled out when considered together.

4.1.2 Basin-scale

Coherent spatial patterns in swe_{peak} climatology are observed in all datasets (Figure 2a), which is consistent with previous work (e.g. Bian et al., 2019 and Orsolini et al, 2019). However, pixel-wise swe_{peak} magnitudes vary significantly across datasets (Figure 2a), so do the basin-integrated volumes (SWE_{peak}; Figure 2b). ERA5 and ERA5-land exhibit the highest SWE_{peak} values in all basins over HMA. These products have the best agreement with the HMASR estimates in the winter westerly-dominated basins (Syr Darya, Amu Darya, and Indus), where the other products all underestimate SWE_{peak} compared to HMASR. MERRA2 consistently shows the least SWE_{peak} across all basins.

In contrast, SWE_{peak} is significantly overestimated in ERA5 and ERA5-land, compared to HMASR, in the monsoon-dominated basins (Salween, Mekong, Yangtze and Yellow), which may be caused by the excess precipitation and lack of melt in its snow model (Orsolini et al., 2019; Hersbach et al., 2020). GLDAS products show the best agreement with HMASR in these basins, followed by JRA55 with comparable or slightly underestimated SWE_{peak} values. This is not surprising as JRA55 assimilates in-situ snow depth observations over the Tibetan Plateau, where most stations are sparsely located in the valleys over the eastern HMA (Bian et al., 2019). As suggested in previous work, JRA55 and GLDAS products have relatively good performance in estimating SWE/snow depth compared to in-situ data (Bian et al., 2019; Orsolini et al., 2019; Wang et al., 2020).

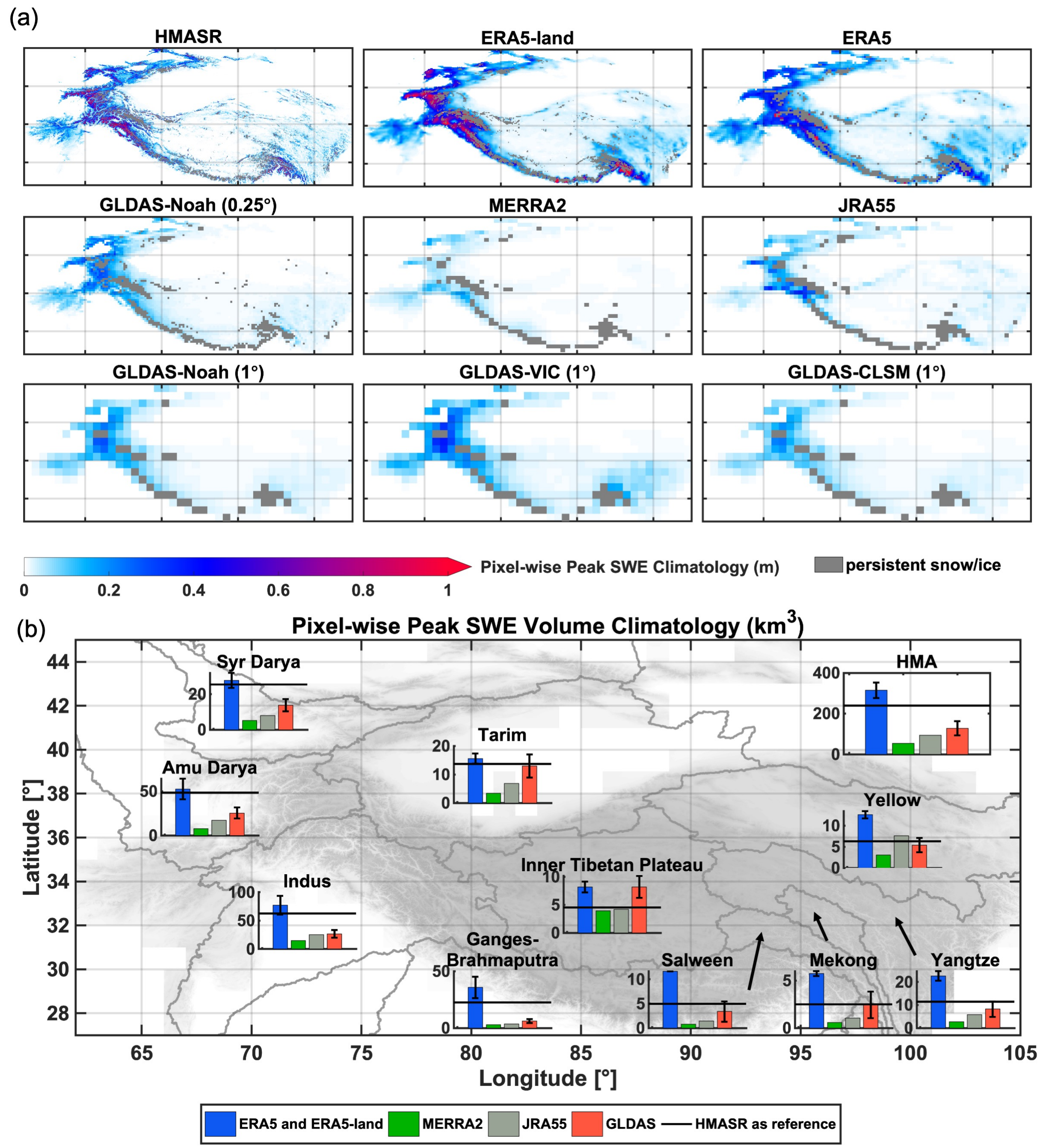

Figure 2. a) The 17-year climatology of pixel-wise peak SWE (swe_{peak}), with persistent snow/ice pixels masked out (gray); **b**) The 17-year climatology of peak SWE volume in each basin (SWE_{peak}, with HMASR SWE shown with horizontal black line). The snow products are grouped into 4 main sets (ERA5 and ERA5-land, MERRA2, JRA55 and GLDAS), with the average SWE_{peak} (bar plot) and the standard deviation (error bars) shown for the ERA5 and GLDAS groups.

4.2 Drivers of peak SWE variations across snow products

4.2.1 Accumulation-season snowfall and ablation

The variability in S_{acc} and A_{acc} climatology among snow products is characterized in Figure 3 to illustrate their relative influence on SWE_{peak} variability. Overall, there exists large variations in S_{acc} and A_{acc} estimates across the existing snow products. S_{acc} is generally the largest in ERA5/ERA5-land products and is the smallest in MERRA2/GLDAS products, with the mean and uncertainty characterized by 335 km^3 $\pm$ 148 km^3 over the entire HMA, 178 km^3 $\pm$ 83 km^3 in seasonal snow regimes and 157 km^3 $\pm$ 67 km^3 in ephemeral snow regimes. A_{acc} and its ratio to S_{acc} are also quite significant and variable across snow products, indicating snow loss via ablation during the accumulation season is a non-negligible factor in determining SWE_{peak}. Specifically, between 40% (ERA5-land) and 65% (MERRA2) of snowfall is lost to ablation during the accumulation season, with the overall ablation loss fraction given by 51% $\pm$ 9%. The snowfall loss to ablation is less in seasonal snow regimes, but the ratio still varies significantly across products (from 17% in ERA5-land to 55% in MERRA2, or 37% $\pm$ 13% across snow products). In ephemeral snow regimes, the snowfall loss to ablation during the accumulation season is large but more consistent across snow products (from 58% in GLDAS-VIC to 76% in MERRA2; 67% $\pm$ 7%). Other work, focused on the WUS has also identified ablation as a significant accumulation-season loss term (Cho et al., 2022).

The elevational distribution of S_{acc}, A_{acc} and SWE_{peak} climatology over the full HMA domain were normalized by total S_{acc} volume to illustrate the volumetric fraction (Figure S4). The distribution in fractional S_{acc} exhibits general consistency across snow products, while the distribution in fractional A_{acc} is significantly more distinct across products. This leads to a distinct distribution in fractional SWE_{peak} rather than just reproducing the fractional S_{acc} distribution, and highlights the important role of ablation in removing snowfall differently with elevation over the accumulation season (Text S8).

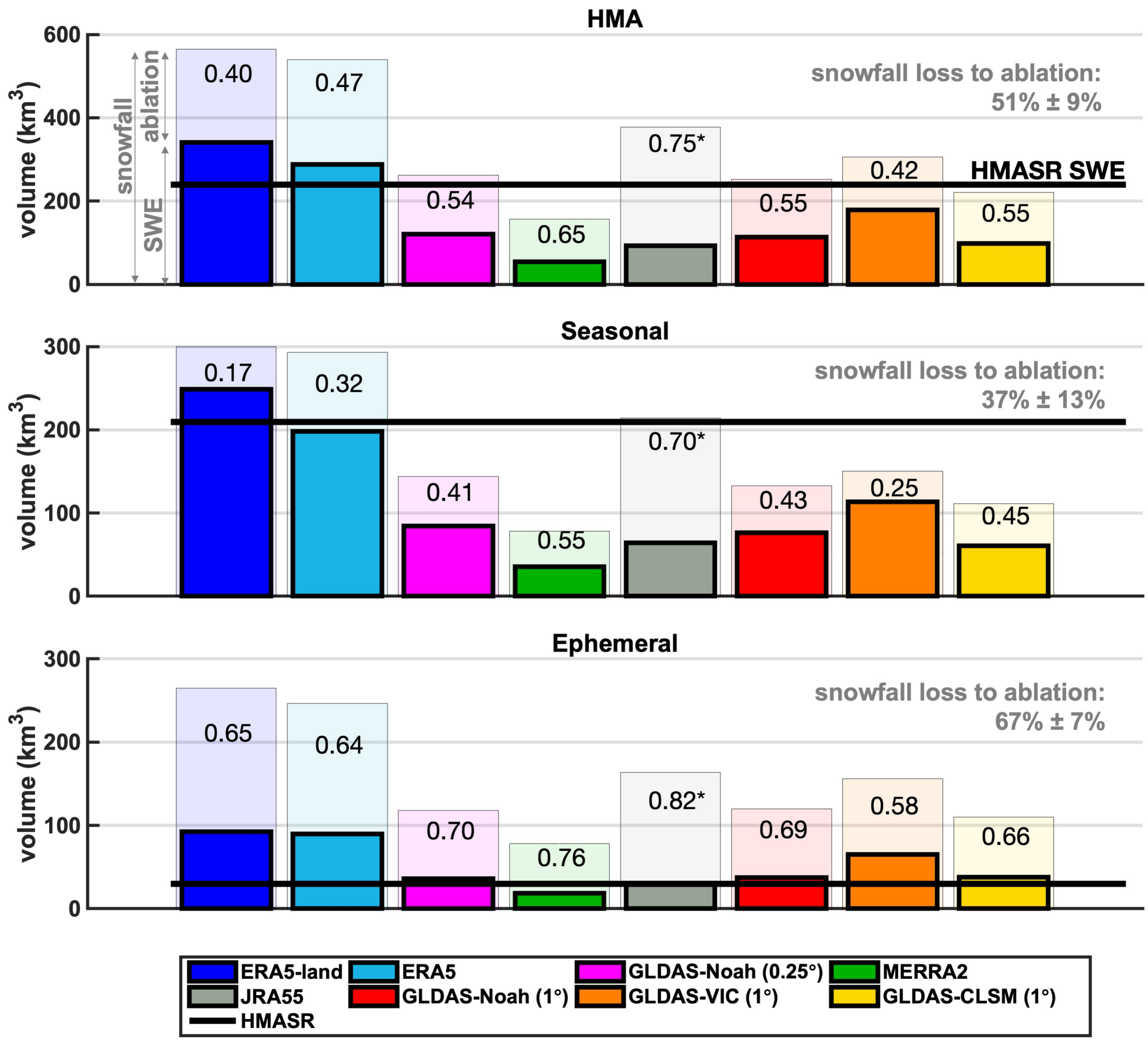

Figure 3. The 17-year climatology of peak SWE volume (SWE_{peak}, solid bars) and accumulation-season snowfall volume (S_{acc}, shaded bars) integrated over HMA (top panel) and areas with seasonal (middle panel) and ephemeral snow (bottom panel). HMASR SWE is provided as a reference (solid black horizontal line). The text labels in each bar plot indicate the fraction of cumulative accumulation-season snowfall lost to ablation. JRA55 ablation fraction is only displayed here (noted with a symbol *) but not included in the discussion due to its diagnosed ablation being overestimated as a result of its snow data assimilation updates (Text S3).

4.2.2 Contributions to peak snow storage variations

To explain peak SWE variations, linear regression (Text S6) was applied across snow products and/or WYs. Over the full HMA domain, a strong linear dependence between the interannual SWE_{peak} and S_{acc} is clear (Figure 4a). Notably, S_{acc} values exhibit a large range (100 – 700 km^3) and have a sizeable gap between GLDAS and ERA5/ERA5-land. The global regression slope (β_{global}; across all snow products) is 0.54, indicating that, during the accumulation season, ~54% of snowfall goes into SWE_{peak}, while the other 46% is lost through ablation. Snowfall's contribution to SWE_{peak} is higher in seasonal snow regimes (Figure 4b), where ~71% of snowfall goes into peak SWE and 29% is lost via ablation. In ephemeral snow regimes (Figure 4c), however, ~35% of snowfall goes into peak SWE while 65% is lost via ablation. These diagnosed fractions from multi-WY and multi-product analysis (Figure 4) are consistent with those derived from the climatology (Figure 3). The coefficient of determination (R^2) is 0.88, 0.88 and 0.80 for the full HMA domain, seasonal snow regime and ephemeral snow regime, respectively. Such values are informative in 1) confirming the expected strong linear dependence of SWE_{peak} and S_{acc} across all datasets and all WYs, and 2) over 80% of SWE_{peak} uncertainty is explained by S_{acc} variability and the other 20% or less is explained by A_{acc} variations.

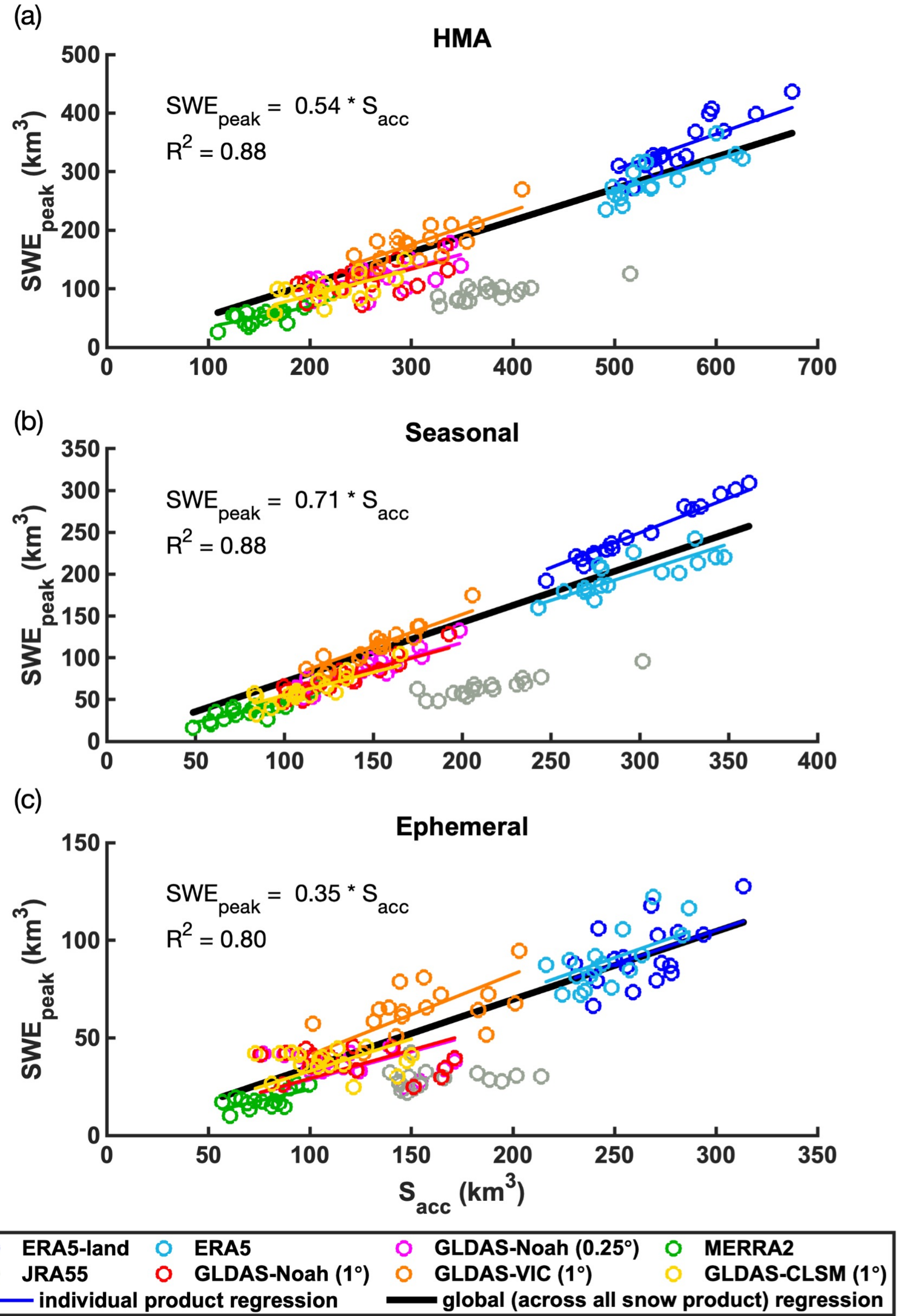

Figure 4. Regression of peak SWE volume (SWE_{peak}) and accumulation-season snowfall (S_{acc}) across all WYs (2001-2017), with volumes integrated over the **a)** the full HMA domain, **b)** seasonal, and **c)** ephemeral snow regimes, respectively. Note that JRA55 is displayed here but is not included in the linear regression due to its diagnosed ablation being overestimated as a result of its snow data assimilation updates.

In addition to treating all datasets as a large sample, we also evaluated the interannual variability for individual snow products and examined product-specific linear regression results. The individual regression slopes are distinct from the global slope value (Figure 4 and Table S4). ERA5-land and GLDAS-VIC exhibit higher slopes, while MERRA2 and the other GLDAS products exhibit lower slopes. The linear dependence of SWE_{peak} and S_{acc} are very strong in seasonal snow (with R^2 ranging from 0.62 to 0.94) but much weaker in ephemeral snow (with R^2 ranging from 0.25 to 0.48) when examining individual snow products (Text S9 and Table S4). This can be attributed to ephemeral snow being more influenced by ablation, introducing additional noise into the snowfall-peak SWE relationship.

Given the large range in S_{acc} across snow products, including the sizeable gap between ERA5/ERA5-land and the other snow products (GLDAS and MERRA2), we also separately regressed SWE_{peak} vs. S_{acc} for these two groups of snow products (Text S9 and Figure S5). In doing so, the R^2 values drop to 58% and 43% respectively (from the global value of 0.88), indicating that A_{acc} is a more important (explaining 42% and 57% of SWE_{peak} uncertainty, respectively) when examined in certain subsets of products.

The results above indicate (not surprisingly) that S_{acc} variations are the primary factor in explaining SWE_{peak} variations in HMA, while ablation plays an important role. To decipher the degree to which those variations are explained by variations in precipitation vs. rain-snow partitioning across snow products, the accumulation-season snowfall volume (S_{acc}) was regressed against precipitation volume (P_{acc}) (Text S9 and Figure S6). S_{acc} shows very high linear dependence on P_{acc} (R^2 up to 0.96), and there is a relatively minor difference when adding accumulation-season air temperature into the regression (R^2 slightly increased to ~0.98). This identifies the key role of precipitation in contributing to SWE_{peak} uncertainties (where similar results are found in Cho et al., 2022 in the WUS), highlighting the top priority of reducing precipitation uncertainties for accurate SWE estimation.

5 Conclusion

Accurate knowledge of peak snow water storage in HMA is a pre-requisite for predicting warm-season runoff, which is critical for the water supply to the large population and agricultural production in downstream areas. Results in this study confirm that our current state of knowledge of this important water resource is highly uncertain. Eight globally available snow products were examined, with the use of HMASR as a reference, to specifically analyze the peak snow storage and how it is affected by accumulation vs. ablation processes during the accumulation season. The key findings are:

1) The integrated pixel-wise peak snow storage (SWE_{peak}) climatology across snow products was found to be 161 km^3 $\pm$ 102 km^3 over HMA, with varying uncertainty levels for seasonal (110 km^3 $\pm$ 74 km^3) vs. ephemeral (51 km^3 $\pm$ 28 km^3) snow. Compared to HMASR, the other snow products on average underestimate SWE_{peak} by 33% (MD) with a RMSD of 52% over the entire HMA. The error and uncertainty vary across different watersheds, where on average, the snow products underestimate seasonal snow (by 47%) and overestimate ephemeral snow (by 70%), compared to HMASR.

2) There exists large variability in the accumulation-season snowfall (S_{acc}) and ablation (A_{acc}) climatology. S_{acc} climatology was found to be 335 km^3 $\pm$ 148 km^3, with 51% $\pm$

9% of the total accumulation-season snowfall lost via ablation prior to the peak snow timing. The fraction differs between seasonal (37% $\pm$ 13%) and ephemeral (67% $\pm$ 7%) snow regimes. Both S_{acc} and A_{acc} play important roles in determining the spatial and elevational distribution in SWE_{peak}.

3) Uncertainty in inter-product peak snow storage estimates over HMA is primarily explained by S_{acc} (88%), with 88% and 80% in seasonal and ephemeral snow regimes respectively. The sensitivity to the chosen snow product ensemble could be a caveat to the relative importance of S_{acc} in explaining SWE_{peak} uncertainty; when the eight datasets are partitioned into two subsets (as separated by the notable gap in S_{acc}), A_{acc} was found to explain more SWE_{peak} variations (42% and 57%, respectively) when examined within each subset.

Reducing accumulation-season uncertainty will be a key first step to properly constraining melt-season processes (i.e. by providing an accurate initial condition of stored snow) that control snowmelt rates, infiltration, and runoff. Reducing the uncertainty in HMA snow storage estimates will require improved characterization of both snowfall and ablation processes and/or better measurements of SWE to constrain models during the accumulation season. The specific drivers for snow ablation variability during the accumulation season are not explored in this work, as they are typically intertwined with individual model physics, but are also important for peak SWE estimation (Cho et al., 2022) and should be investigated in future work.

Acknowledgments

We would like to thank those responsible for the creation of the datasets used in this study. This research was funded by the NASA High-Mountain Asia Program Grant #NNX16AQ63G with additional support provided by NSF Grant #1641960.

Open Research

Data Availability Statement

The HMASR dataset used in this work is publicly available on National Snow and Ice Data Center (NSIDC; https://doi.org/10.5067/HNAUGJQXSCVU). Other global reanalysis products are also acquired online: ERA5 and ERA5-land data are obtained from the Copernicus Climate Change Service (C3S) Climate Date Store (ERA5: https://doi.org/10.24381/cds.adbb2d47; ERA5-land: https://doi.org/10.24381/cds.e2161bac). JRA55 is downloaded from: http://search.diasjp.net/en/dataset/JRA55.

MERRA2 data is obtained from the NASA Goddard Earth Sciences Data and Information Service Center (GES DISC; https://disc.gsfc.nasa.gov/), with the specification of SWE (SNOMAS) obtained from https://doi.org/10.5067/RKPHT8KC1Y1T, bias-corrected precipitation (PRECTOTCORR) obtained from https://doi.org/10.5067/7MCPBJ41Y0K6, bias-corrected snowfall (PRECSNOCORR) from https://doi.org/10.5067/L0T5GEG1NYFA, air temperature (T2M) from https://doi.org/10.5067/VJAFPLI1CSIV.

GLDAS datasets are also obtained from GES DISC (GLDAS-2.1 version is used in this work), as follows: GLDAS-Noah (0.25°) is acquired from https://doi.org/10.5067/E7TYRXPJKWOQ; GLDAS-Noah (1°) is acquired from https://doi.org/10.5067/IIG8FHR17DA9; GLDAS-VIC (1°) is acquired from https://doi.org/10.5067/ZOG6BCSE26HV; and GLDAS-CLSM (1°) is acquired from https://doi.org/10.5067/VCO8OCV72XO0.

References

Armstrong, R. L., Rittger, K., Brodzik, M. J., Racoviteanu, A., Barrett, A. P., Khalsa, S.-J. S., Raup, B., Hill, A. F., Khan, A. L., Wilson, A. M., Kayastha, R. B., Fetterer, F., & Armstrong, B. (2019). Runoff from glacier ice and seasonal snow in High Asia: Separating melt water sources in river flow. *Regional Environmental Change*, *19*(5), 1249–1261. https://doi.org/10.1007/s10113-018-1429-0

Bian, Q., Xu, Z., Zhao, L., Zhang, Y.-F., Zheng, H., Shi, C., Zhang, S., Xie, C., & Yang, Z.-L. (2019). Evaluation and Intercomparison of Multiple Snow Water Equivalent Products over the Tibetan Plateau. *Journal of Hydrometeorology*, *20*(10), 2043–2055. https://doi.org/10.1175/JHM-D-19-0011.1

Bookhagen, B., & Burbank, D. W. (2010). Toward a complete Himalayan hydrological budget: Spatiotemporal distribution of snowmelt and rainfall and their impact on river discharge. *Journal of Geophysical Research: Earth Surface*, *115*(F3). https://doi.org/10.1029/2009JF001426

Bormann, K. J., Brown, R. D., Derksen, C., & Painter, T. H. (2018). Estimating snow-cover trends from space. *Nature Climate Change*, *8*(11), 924–928. https://doi.org/10.1038/s41558-018-0318-3

Cho, E., Vuyovich, C. M., Kumar, S. V., Wrzesien, M. L., Kim, R. S., & Jacobs, J. M. (2022). Precipitation Biases and Snow Physics Limitations Drive the Uncertainties in Macroscale Modeled Snow Water Equivalent. *Hydrology and Earth System Sciences Discussions*, *2022*, 1–22. https://doi.org/10.5194/hess-2022-136

Dozier, J., Bair, E. H., & Davis, R. E. (2016). Estimating the spatial distribution of snow water equivalent in the world's mountains. *WIREs Water*, *3*(3), 461–474. https://doi.org/10.1002/wat2.1140

Gelaro, R., McCarty, W., Suárez, M. J., Todling, R., Molod, A., Takacs, L., Randles, C. A., Darmenov, A., Bosilovich, M. G., Reichle, R., Wargan, K., Coy, L., Cullather, R., Draper, C., Akella, S., Buchard, V., Conaty, A., da Silva, A. M., Gu, W., … Zhao, B. (2017). The Modern-Era Retrospective Analysis for Research and Applications, Version 2 (MERRA-2). *Journal of Climate*, *30*(14), 5419–5454. https://doi.org/10.1175/JCLI-D-16-0758.1

Hersbach, H., Bell, B., Berrisford, P., Hirahara, S., Horányi, A., Muñoz-Sabater, J., Nicolas, J., Peubey, C., Radu, R., Schepers, D., Simmons, A., Soci, C., Abdalla, S., Abellan, X., Balsamo, G., Bechtold, P., Biavati, G., Bidlot, J., Bonavita, M., … Thépaut, J.-N. (2020).

The ERA5 global reanalysis. *Quarterly Journal of the Royal Meteorological Society*, *146*(730), 1999–2049. https://doi.org/10.1002/qj.3803

Huning, L. S., & AghaKouchak, A. (2020). Global snow drought hot spots and characteristics. *Proceedings of the National Academy of Sciences*, *117*(33), 19753. https://doi.org/10.1073/pnas.1915921117

Immerzeel, W. W., Lutz, A. F., Andrade, M., Bahl, A., Biemans, H., Bolch, T., Hyde, S., Brumby, S., Davies, B. J., Elmore, A. C., Emmer, A., Feng, M., Fernández, A., Haritashya, U., Kargel, J. S., Koppes, M., Kraaijenbrink, P. D. A., Kulkarni, A. V., Mayewski, P. A., … Baillie, J. E. M. (2020). Importance and vulnerability of the world's water towers. *Nature*, *577*(7790), 364–369. https://doi.org/10.1038/s41586-019-1822-y

Immerzeel, W. W., van Beek, L. P. H., & Bierkens, M. F. P. (2010). Climate Change Will Affect the Asian Water Towers. *Science*, *328*(5984), 1382. https://doi.org/10.1126/science.1183188

Khanal, S., Lutz, A. F., Kraaijenbrink, P. D. A., van den Hurk, B., Yao, T., & Immerzeel, W. W. (2021). Variable 21st Century Climate Change Response for Rivers in High Mountain Asia at Seasonal to Decadal Time Scales. *Water Resources Research*, *57*(5), e2020WR029266. https://doi.org/10.1029/2020WR029266

Kim, R. S., Kumar, S., Vuyovich, C., Houser, P., Lundquist, J., Mudryk, L., Durand, M., Barros, A., Kim, E. J., Forman, B. A., Gutmann, E. D., Wrzesien, M. L., Garnaud, C., Sandells, M., Marshall, H.-P., Cristea, N., Pflug, J. M., Johnston, J., Cao, Y., … Wang, S. (2021). Snow Ensemble Uncertainty Project (SEUP): Quantification of snow water equivalent uncertainty across North America via ensemble land surface modeling. *The Cryosphere*, *15*(2), 771–791. https://doi.org/10.5194/tc-15-771-2021

KOBAYASHI, S., OTA, Y., HARADA, Y., EBITA, A., MORIYA, M., ONODA, H., ONOGI, K., KAMAHORI, H., KOBAYASHI, C., ENDO, H., MIYAOKA, K., & TAKAHASHI, K. (2015). The JRA-55 Reanalysis: General Specifications and Basic Characteristics. *Journal of the Meteorological Society of Japan. Ser. II*, *93*(1), 5–48. https://doi.org/10.2151/jmsj.2015-001

Kraaijenbrink, P. D. A., Stigter, E. E., Yao, T., & Immerzeel, W. W. (2021). Climate change decisive for Asia's snow meltwater supply. *Nature Climate Change*, *11*(7), 591–597. https://doi.org/10.1038/s41558-021-01074-x

Lehner, B., Verdin, K., & Jarvis, A. (2008). New Global Hydrography Derived From Spaceborne Elevation Data. *Eos, Transactions American Geophysical Union*, *89*(10), 93–94. https://doi.org/10.1029/2008EO100001

Li, D., Lettenmaier, D. P., Margulis, S. A., & Andreadis, K. (2019). The Value of Accurate High-Resolution and Spatially Continuous Snow Information to Streamflow Forecasts. *Journal of Hydrometeorology*, *20*(4), 731–749. https://doi.org/10.1175/JHM-D-18-0210.1

Liston, G. E., & Elder, K. (2006). A Distributed Snow-Evolution Modeling System (SnowModel). *Journal of Hydrometeorology*, *7*(6), 1259–1276. https://doi.org/10.1175/JHM548.1

Liu, Y., Fang, Y., & Margulis, S.A. (2021a). High Mountain Asia UCLA Daily Snow Reanalysis, Version 1. Boulder, Colorado USA, NASA Snow and Ice Data Center Distributed Active Archive Center. https://doi.org/10.5067/HNAUGJQXSCVU

Liu, Y., Fang, Y., & Margulis, S. A. (2021b). Spatiotemporal distribution of seasonal snow water equivalent in High Mountain Asia from an 18-year Landsat–MODIS era snow reanalysis dataset. *The Cryosphere*, *15*(11), 5261–5280. https://doi.org/10.5194/tc-15-5261-2021

Mankin, J. S., Viviroli, D., Singh, D., Hoekstra, A. Y., & Diffenbaugh, N. S. (2015). The potential for snow to supply human water demand in the present and future. *Environmental Research Letters*, *10*(11), 114016. https://doi.org/10.1088/1748-9326/10/11/114016

McCrary, R. R., & Mearns, L. O. (2019). Quantifying and Diagnosing Sources of Uncertainty in Midcentury Changes in North American Snowpack from NARCCAP. *Journal of Hydrometeorology*, *20*(11), 2229–2252. https://doi.org/10.1175/JHM-D-18-0248.1

Mortimer, C., Mudryk, L., Derksen, C., Luojus, K., Brown, R., Kelly, R., & Tedesco, M. (2020). Evaluation of long-term Northern Hemisphere snow water equivalent products. *The Cryosphere*, *14*(5), 1579–1594. https://doi.org/10.5194/tc-14-1579-2020

Mudryk, L. R., Derksen, C., Kushner, P. J., & Brown, R. (2015). Characterization of Northern Hemisphere Snow Water Equivalent Datasets, 1981–2010. *Journal of Climate*, *28*(20), 8037–8051. https://doi.org/10.1175/JCLI-D-15-0229.1

Muñoz-Sabater, J., Dutra, E., Agustí-Panareda, A., Albergel, C., Arduini, G., Balsamo, G., Boussetta, S., Choulga, M., Harrigan, S., Hersbach, H., Martens, B., Miralles, D. G., Piles, M., Rodríguez-Fernández, N. J., Zsoter, E., Buontempo, C., & Thépaut, J.-N. (2021). ERA5-Land: A state-of-the-art global reanalysis dataset for land applications. *Earth System Science Data*, *13*(9), 4349–4383. https://doi.org/10.5194/essd-13-4349-2021

Orsolini, Y., Wegmann, M., Dutra, E., Liu, B., Balsamo, G., Yang, K., de Rosnay, P., Zhu, C., Wang, W., Senan, R., & Arduini, G. (2019). Evaluation of snow depth and snow cover over the Tibetan Plateau in global reanalyses using in situ and satellite remote sensing observations. *The Cryosphere*, *13*(8), 2221–2239. https://doi.org/10.5194/tc-13-2221-2019

Palazzi, E., Hardenberg, J., & Provenzale, A. (2013). Precipitation in the Hindu-Kush Karakoram Himalaya: Observations and future scenarios. *Journal of Geophysical Research: Atmospheres*, *118*(1), 85–100. https://doi.org/10.1029/2012JD018697

Petersky, R., & Harpold, A. (2018). Now you see it, now you don't: A case study of ephemeral snowpacks and soil moisture response in the Great Basin, USA. *Hydrology and Earth System Sciences*, *22*(9), 4891–4906. https://doi.org/10.5194/hess-22-4891-2018

Qin, Y., Abatzoglou, J. T., Siebert, S., Huning, L. S., AghaKouchak, A., Mankin, J. S., Hong, C., Tong, D., Davis, S. J., & Mueller, N. D. (2020). Agricultural risks from changing snowmelt. *Nature Climate Change*, *10*(5), 459–465. https://doi.org/10.1038/s41558-020-0746-8

Rodell, M., Houser, P. R., Jambor, U., Gottschalck, J., Mitchell, K., Meng, C.-J., Arsenault, K., Cosgrove, B., Radakovich, J., Bosilovich, M., Entin, J. K., Walker, J. P., Lohmann, D., & Toll, D. (2004). The Global Land Data Assimilation System. *Bulletin of the American Meteorological Society*, *85*(3), 381–394. https://doi.org/10.1175/BAMS-85-3-381

Sturm, M., Holmgren, J., & Liston, G. E. (1995). A Seasonal Snow Cover Classification System for Local to Global Applications. *Journal of Climate*, *8*(5), 1261–1283. https://doi.org/10.1175/1520-0442(1995)008<1261:ASSCCS>2.0.CO;2

Terzago, S., von Hardenberg, J., Palazzi, E., & Provenzale, A. (2014). Snowpack Changes in the Hindu Kush–Karakoram–Himalaya from CMIP5 Global Climate Models. *Journal of Hydrometeorology*, *15*(6), 2293–2313. https://doi.org/10.1175/JHM-D-13-0196.1

Viviroli, D., Dürr, H. H., Messerli, B., Meybeck, M., & Weingartner, R. (2007). Mountains of the world, water towers for humanity: Typology, mapping, and global significance. *Water Resources Research*, *43*(7). https://doi.org/10.1029/2006WR005653

Wang, X., Tolksdorf, V., Otto, M., & Scherer, D. (2020). WRF-based dynamical downscaling of ERA5 reanalysis data for High Mountain Asia: Towards a new version of the High Asia Refined analysis. *International Journal of Climatology*, *41*(1), 743–762. https://doi.org/10.1002/joc.6686

Wrzesien, M. L., Pavelsky, T. M., Durand, M. T., Dozier, J., & Lundquist, J. D. (2019). Characterizing Biases in Mountain Snow Accumulation From Global Data Sets. *Water Resources Research*, *55*(11), 9873–9891. https://doi.org/10.1029/2019WR025350

Xiao, L., Che, T., & Dai, L. (2020). Evaluation of Remote Sensing and Reanalysis Snow Depth Datasets over the Northern Hemisphere during 1980–2016. *Remote Sensing*, *12*(19). https://doi.org/10.3390/rs12193253

Xu, Y., Jones, A., & Rhoades, A. (2019). A quantitative method to decompose SWE differences between regional climate models and reanalysis datasets. *Scientific Reports*, *9*(1), 16520. https://doi.org/10.1038/s41598-019-52880-5

Yao, T., Thompson, L., Yang, W., Yu, W., Gao, Y., Guo, X., Yang, X., Duan, K., Zhao, H., Xu, B., Pu, J., Lu, A., Xiang, Y., Kattel, D. B., & Joswiak, D. (2012). Different glacier status with atmospheric circulations in Tibetan Plateau and surroundings. *Nature Climate Change*, *2*(9), 663–667. https://doi.org/10.1038/nclimate1580

References from the supporting information

Bian, Q., Xu, Z., Zhao, L., Zhang, Y.-F., Zheng, H., Shi, C., Zhang, S., Xie, C., & Yang, Z.-L. (2019). Evaluation and Intercomparison of Multiple Snow Water Equivalent Products over the Tibetan Plateau. *Journal of Hydrometeorology*, *20*(10), 2043–2055. https://doi.org/10.1175/JHM-D-19-0011.1

Cho, E., Vuyovich, C. M., Kumar, S. V., Wrzesien, M. L., Kim, R. S., & Jacobs, J. M. (2022). Precipitation Biases and Snow Physics Limitations Drive the Uncertainties in Macroscale Modeled Snow Water Equivalent. *Hydrology and Earth System Sciences Discussions*, *2022*, 1–22. https://doi.org/10.5194/hess-2022-136

Clark, M. P., Hendrikx, J., Slater, A. G., Kavetski, D., Anderson, B., Cullen, N. J., Kerr, T., Örn Hreinsson, E., & Woods, R. A. (2011). Representing spatial variability of snow water equivalent in hydrologic and land-surface models: A review. *Water Resources Research*, *47*(7). https://doi.org/10.1029/2011WR010745

Gelaro, R., McCarty, W., Suárez, M. J., Todling, R., Molod, A., Takacs, L., Randles, C. A., Darmenov, A., Bosilovich, M. G., Reichle, R., Wargan, K., Coy, L., Cullather, R., Draper, C., Akella, S., Buchard, V., Conaty, A., da Silva, A. M., Gu, W., … Zhao, B. (2017). The Modern-Era Retrospective Analysis for Research and Applications, Version 2 (MERRA-2). *Journal of Climate*, *30*(14), 5419–5454. https://doi.org/10.1175/JCLI-D-16-0758.1

Hersbach, H., Bell, B., Berrisford, P., Hirahara, S., Horányi, A., Muñoz-Sabater, J., Nicolas, J., Peubey, C., Radu, R., Schepers, D., Simmons, A., Soci, C., Abdalla, S., Abellan, X., Balsamo, G., Bechtold, P., Biavati, G., Bidlot, J., Bonavita, M., … Thépaut, J.-N. (2020). The ERA5 global reanalysis. *Quarterly Journal of the Royal Meteorological Society*, *146*(730), 1999–2049. https://doi.org/10.1002/qj.3803

KOBAYASHI, S., OTA, Y., HARADA, Y., EBITA, A., MORIYA, M., ONODA, H., ONOGI, K., KAMAHORI, H., KOBAYASHI, C., ENDO, H., MIYAOKA, K., & TAKAHASHI, K. (2015). The JRA-55 Reanalysis: General Specifications and Basic Characteristics. *Journal of the Meteorological Society of Japan. Ser. II*, *93*(1), 5–48. https://doi.org/10.2151/jmsj.2015-001

Liu, Y., Fang, Y., & Margulis, S.A. (2021a). High Mountain Asia UCLA Daily Snow Reanalysis, Version 1. Boulder, Colorado USA, NASA Snow and Ice Data Center Distributed Active Archive Center. https://doi.org/10.5067/HNAUGJQXSCVU

Liu, Y., Fang, Y., & Margulis, S. A. (2021b). Spatiotemporal distribution of seasonal snow water equivalent in High Mountain Asia from an 18-year Landsat–MODIS era snow reanalysis dataset. *The Cryosphere*, *15*(11), 5261–5280. https://doi.org/10.5194/tc-15-5261-2021

Magnusson, J., Wever, N., Essery, R., Helbig, N., Winstral, A., & Jonas, T. (2015). Evaluating snow models with varying process representations for hydrological applications. *Water Resources Research*, *51*(4), 2707–2723. https://doi.org/10.1002/2014WR016498

Muñoz-Sabater, J., Dutra, E., Agustí-Panareda, A., Albergel, C., Arduini, G., Balsamo, G., Boussetta, S., Choulga, M., Harrigan, S., Hersbach, H., Martens, B., Miralles, D. G., Piles, M., Rodríguez-Fernández, N. J., Zsoter, E., Buontempo, C., & Thépaut, J.-N. (2021). ERA5-Land: A state-of-the-art global reanalysis dataset for land applications. *Earth System Science Data*, *13*(9), 4349–4383. https://doi.org/10.5194/essd-13-4349-2021

ONOGI, K., TSUTSUI, J., KOIDE, H., SAKAMOTO, M., KOBAYASHI, S., HATSUSHIKA, H., MATSUMOTO, T., YAMAZAKI, N., KAMAHORI, H., TAKAHASHI, K., KADOKURA, S., WADA, K., KATO, K., OYAMA, R., OSE, T., MANNOJI, N., & TAIRA, R. (2007). The JRA-25 Reanalysis. *気象集誌. 第 2 輯*, *85*(3), 369–432. https://doi.org/10.2151/jmsj.85.369

Petersky, R., & Harpold, A. (2018). Now you see it, now you don’t: A case study of ephemeral snowpacks and soil moisture response in the Great Basin, USA. *Hydrology and Earth System Sciences*, *22*(9), 4891–4906. https://doi.org/10.5194/hess-22-4891-2018

Reichle, R. H., Draper, C. S., Liu, Q., Girotto, M., Mahanama, S. P. P., Koster, R. D., & De Lannoy, G. J. M. (2017). Assessment of MERRA-2 Land Surface Hydrology Estimates. *Journal of Climate*, *30*(8), 2937–2960. https://doi.org/10.1175/JCLI-D-16-0720.1

Rodell, M., Houser, P. R., Jambor, U., Gottschalck, J., Mitchell, K., Meng, C.-J., Arsenault, K., Cosgrove, B., Radakovich, J., Bosilovich, M., Entin, J. K., Walker, J. P., Lohmann, D., & Toll, D. (2004). The Global Land Data Assimilation System. *Bulletin of the American Meteorological Society*, *85*(3), 381–394. https://doi.org/10.1175/BAMS-85-3-381

Sturm, M., Holmgren, J., & Liston, G. E. (1995). A Seasonal Snow Cover Classification System for Local to Global Applications. *Journal of Climate*, *8*(5), 1261–1283. https://doi.org/10.1175/1520-0442(1995)008<1261:ASSCCS>2.0.CO;2

Wrzesien, M. L., Pavelsky, T. M., Durand, M. T., Dozier, J., & Lundquist, J. D. (2019). Characterizing Biases in Mountain Snow Accumulation From Global Data Sets. *Water Resources Research*, *55*(11), 9873–9891. https://doi.org/10.1029/2019WR025350

Xu, Y., Jones, A., & Rhoades, A. (2019). A quantitative method to decompose SWE differences between regional climate models and reanalysis datasets. *Scientific Reports*, *9*(1), 16520. https://doi.org/10.1038/s41598-019-52880-5

Geophysical Research Letters

Supporting Information for

How well do we characterize snow storage in High Mountain Asia?

Yufei Liu[1], Yiwen Fang[1], Dongyue Li[1] and Steven A. Margulis[1]

Department of Civil and Environmental Engineering, University of California, Los Angeles, Los Angeles, CA, 90095

Contents of this file

Text S1 to S9
Figures S1 to S6
Tables S1 to S4

Introduction

This supporting information provides more details on the data, methods and results presented in the main text. Text S1 and Table S1 give details on HMASR and the eight global snow products examined for the intercomparison. Text S2 to Text S6 (along with Table S2 and Figure S1 to Figure S3) provide more clarifications on the methods. Text S7 to Text S9 (along with Table S3 to Table S4; Figure S4 to Figure S6) provide supplementary information for the results.

Text S1. Data: Description of HMASR and eight global snow products

The High Mountain Asia Snow Reanalysis (HMASR) and the eight global snow products are evaluated in this research. Characteristics for each dataset are summarized in Table S1 with details provided as follows:

HMASR (Liu et al., 2021a) is a snow-specific reanalysis dataset, providing daily estimates of SWE at 1/225° (~500 m) resolution, available from Water Years (WYs) 2000 to 2017. Among all datasets examined in this work, HMASR is unique as it was specifically designed for snow estimation in HMA, leveraging remotely sensed fractional snow-covered area (fSCA) and an advanced ensemble-based data assimilation framework. It is directly constrained by snow observations, offering the potential of SWE evaluation at high elevations and over complex terrain, where in-situ stations do not exist.

ERA5 (Hersbach et al., 2020) is the 5th generation product of ECMWF's atmospheric reanalyses that provides hourly estimates at 0.25° resolution. Both in-situ snow depth observations and binary snow cover data from the Interactive Multi-Sensor Snow and Ice Mapping System (IMS) are used in its snow data assimilation (optimal interpolation) system, where snow cover is not used at elevations above 1500 m in the ERA5 snow scheme (Bian et al., 2019). In addition to the ERA5 product itself, the ERA5-land (Muñoz-Sabater et al., 2021) dataset at finer resolution (0.1°) is derived from the same ERA5 forcing and Land Surface model (LSM), but without data assimilation.

MERRA2 (Gelaro et al., 2017) is the 2nd version of NASA's Global Modeling and Assimilation Office (GMAO) reanalysis product, providing hourly estimates at 0.625° x 0.5° resolution. The Catchment model (CLSM) is used as the LSM and no snow data assimilation is performed. MERRA2 uses a bias-corrected precipitation field for precipitation inputs (Reichle et al., 2017) to derive its land surface state estimates including SWE.

JRA55 (Kobayashi et al., 2015) is the latest version of the Japan Meteorology Agency (JMA) reanalysis product that provides sub-daily (e.g. 3-hour snowfall and 6-hour SWE and air temperature) estimates. We selected its highest resolution (~0.5625° x 0.5616°) outputs for this work. JRA55 uses the Simple Biosphere (SiB) model as the LSM in deriving its estimates. Station observed snow depth and satellite retrieved binary snow cover from the Special Sensor Microwave/Imager (SSM/I) and Special Sensor Microwave Imager Sounder (SSMIS) are used to update snow depth using the data assimilation (optimal interpolation) method. SWE estimates are converted from snow depth estimates by assuming a constant snow density (200 kg/m^3; Onogi et al., 2007). The JRA55 product assimilates snow depth data from the stations over the Tibetan Plateau, while ERA5 does not (Onogi et al., 2007; Bian et al., 2019; Orsolini et al., 2019).

GLDAS-2.1 (Rodell et al., 2004) is a global land data assimilation product generated by the NASA Goddard Space Flight Center, providing estimates at sub-daily (3-hour) and 0.25° or 1° resolution, available from January 2000 to present. It contains four datasets: two Noah model driven datasets at 0.25° and 1° resolution, one Variable Infiltration Capacity (VIC) model driven dataset at 1° resolution, and one Catchment (CLSM) model driven dataset at 1° resolution, denoted as GLDAS-Noah (0.25°), GLDAS-Noah (1°), GLDAS-VIC (1°) and GLDAS-CLSM (1°) hereafter. All of the GLDAS-2.1 products are generated using the same set of meteorological forcing inputs, without any snow data assimilation.

Table S1. Characteristics of the snow data products used in this study. For the globally available snow products, in addition to SWE, other forcing variables such as precipitation (*P*), air temperature (T_a) and snowfall (*S*) are also used. [1] Liu et al., 2021a; [2] Muñoz-Sabater et al., 2021; [3] Hersbach et al., 2020; [4] Rodell et al., 2004; [5] Gelaro et al., 2017; [6] Kobayashi et al., 2015

Dataset	**Spatial resolution**	**Temporal coverage**	**Temporal resolution**	**Land Surface Model**	**Assimilated snow observations**	**Available variables used in analysis**
HMASR[1] (reference)	1/225° x 1/225°	1999/10 -2017/09	Daily	SSiB3	Fractional snow-covered area from Landsat and MODSCAG	SWE
ERA5-Land[2]	0.1° x 0.1°	1950 - present	Hourly	H-TESSEL	-	SWE, *P*, T_a, *S*
ERA5[3]	0.25° x 0.25°	1950 - present	Hourly	H-TESSEL	In situ snow depth; IMS snow cover (binary)	SWE, *P*, T_a, *S*
GLDAS-Noah (0.25°)[4]	0.25° x 0.25°	2000/01 - present	3-hour	Noah	-	SWE, *P*, T_a, *S*
MERRA2[5]	0.625° x 0.5°	1979 - present	Hourly	Catchment	-	SWE, *P*, T_a, *S*
JRA-55[6]	0.5625° x 0.5616°	1958 - present	3- or 6-hour	SiB	In-situ snow depth, SSM/I, SSMIS snow cover (binary)	SWE, *P*, T_a, *S*
GLDAS-Noah (1°)	1° x 1°	2000/01 - present	3-hour	Noah	-	SWE, *P*, T_a, *S*
GLDAS-VIC (1°)				VIC		
GLDAS-CLSM (1°)				Catchment		

Text S2. Methods: Definition of the snow accumulation season

The snow accumulation season is defined at the pixel scale, from day of water year (DOWY) 1 (t_0) through the pixel-wise peak SWE DOWY (t_{peak}; Figure S1). Defining these quantities at the pixel-scale isolates accumulation-season processes, while doing so at the basin or larger scale inevitably mixes accumulation season and melt season processes due to significant elevational variations within the region examined. Spatial variations in t_{peak} are indicative of seasonal and elevational patterns in climatology, but are also a function of model-specific inputs and process representation.

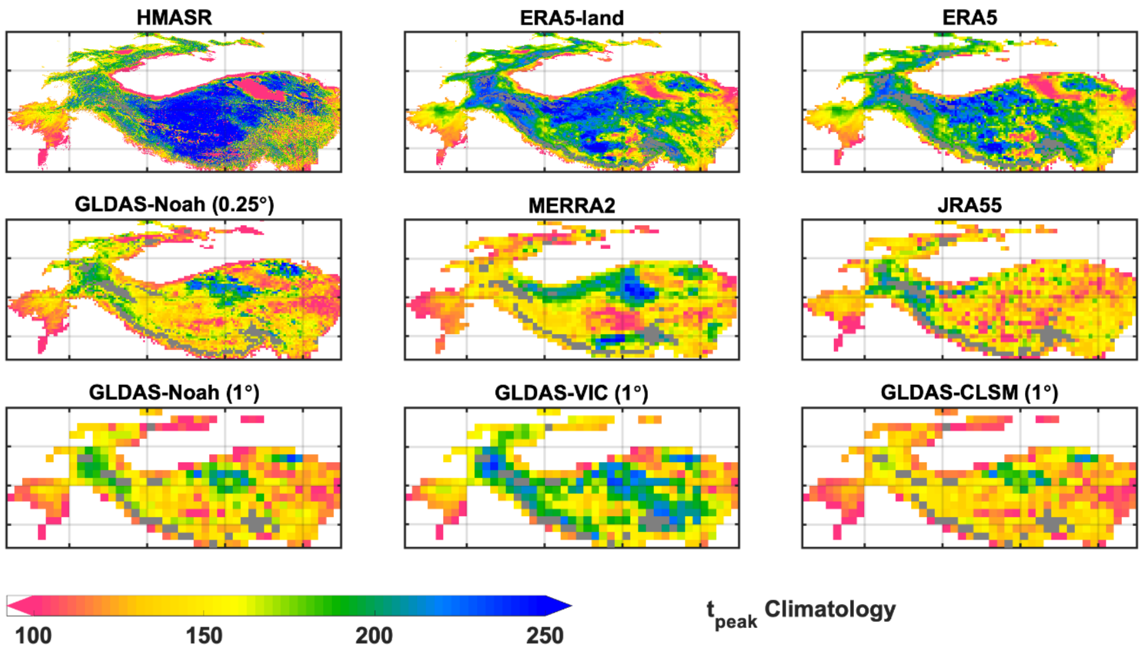

Figure S1. Maps of the 17-year climatology of pixel-wise peak SWE DOWY ($\boldsymbol{t_{peak}}$) for each dataset.

Text S3. Methods: Snow mass balance at the pixel-scale during accumulation season

Snow mass balance at the model pixel scale can be described as the relationship between SWE (denoted as *swe* in m), snowfall (*s*, in m/day) and ablation (*a*, in m/day):

$$\frac{d}{dt} swe = s - a \tag{S1}$$

The snow accumulation season is defined at the pixel scale, from day of water year (DOWY) 1 (t_0) through the pixel-wise peak SWE DOWY (t_{peak}; Figure S2):

$$\int_{t_0}^{t_{peak}} \left[\frac{d}{dt} swe\right] dt = \int_{t_0}^{t_{peak}} [s - a] dt \tag{S2}$$

$$swe_{peak} = s_{acc} - a_{acc} \tag{S3}$$

where swe_{peak} characterizes the net added SWE within the accumulation season at a specific pixel. The s_{acc} and a_{acc} terms denote the cumulative snowfall and snow ablation integrated over the accumulation season. The variables swe_{peak} and s_{acc} are directly obtained from each snow product. Since different LSMs across products represent and handle ablation processes differently, a_{acc} is obtained herein as the difference between s_{acc} and swe_{peak} (similar to Xu et al., 2019):

$$a_{acc} = s_{acc} - swe_{peak} \tag{S4}$$

It should also be noted that while most snow products showed consistency between integrated positive SWE increments and snowfall (Figure 1b in the main text), JRA55 consistently exhibits SWE changes lower than expected relative to snowfall (i.e. data assimilation increments appear to be mostly negative). For this reason, the diagnosed ablation (defined herein as the difference between s_{acc} and swe_{peak}; Equation S4) for JRA55 is likely a mix of model-specific ablation processes and non-negligible data assimilation corrections. This explains why JRA55 has higher snowfall estimates, but among the lower SWE estimates among the datasets in Figure 1b.

Text S4. Methods: Seasonal, ephemeral, and persistent snow masks

As in Liu et al. (2021b), the HMASR dataset is used to derive masks for persistent snow/ice, seasonal snow, and ephemeral (intermittent) snow (Figure S2). The persistent snow mask (derived in Liu et al., 2021b) is used to remove areas that are likely glacierized or with significant carry-over snow storage from one WY to the next. Seasonal and ephemeral snow pixels are distinguished using a threshold of 0.05 m in climatological peak SWE, where the distinction is made due to the expected differences in their accumulation-season characteristics (e.g. seasonal snow lasts longer, ephemeral snow is intermittent with shorter duration, and the latter does not have a distinct accumulation season). Other work uses the Sturm et al. (1995) classification that identifies ephemeral snow as that with the snow duration less than 60 days and snow depth below 50 cm (e.g. Petersky and Harpold, 2018; Wrzesien et al., 2019).

For the purpose of assessing the peak snow storage in HMA, seasonal snow is emphasized in this work. Ephemeral snow is also assessed due to its vast coverage and non-negligible volumetric contribution to the total storage. Both are examined in this work so that the accumulation/ablation processes in the accumulation season are properly characterized for each snow regime. Moreover, areas under 1500 m elevation are screened out within the whole HMA domain and in all three masks (seasonal, ephemeral and persistent snow), to emphasize the focus on areas that are more likely to have snow (above 1500 m elevation).

For consistency, we applied the three HMASR-derived masks to all other datasets, by aggregating them from the original HMASR resolution (~500 m) to the coarser resolution grids in each product (Figure S2). The masked areas were carefully examined to make sure they are comparable across datasets (Table S2). Seasonal snow regimes mainly cover the northwestern mountain regions (dominated by winter westerlies, covering ~23% of the total area), while ephemeral snow mainly covers the vast area in the central and eastern regions (dominated by summer monsoons, covering ~69% of the total area), with the highest mountains covered by persistent snow/ice (covering ~8% of the total area).

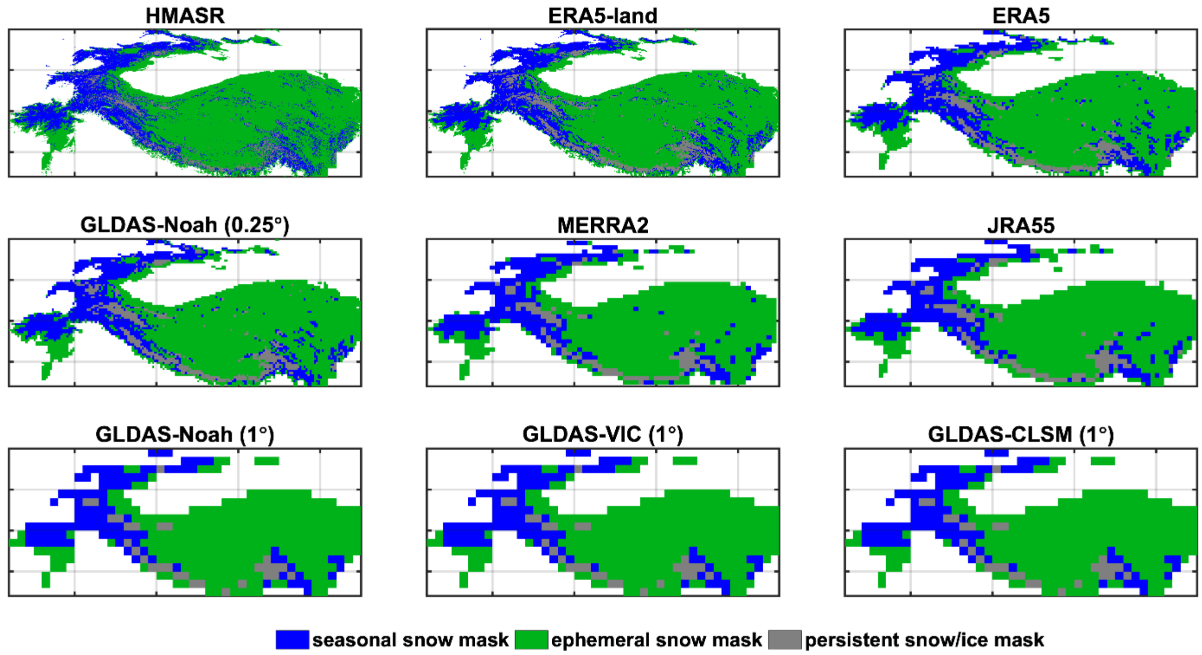

Figure S2. The derived seasonal snow, ephemeral snow, and persistent snow/ice masks shown at the native resolution of each dataset.

Table S2. The total domain area (above 1500 m elevation) and the area of seasonal snow, ephemeral snow, and persistent snow/ice in all datasets.

Dataset	Total Domain Area (above 1500 m elevation) (10^6 km^2)	Seasonal Snow Area (10^6 km^2)	Ephemeral Snow Area (10^6 km^2)	Persistent snow/ice area (10^6 km^2)
HMASR	4.14	1.00	2.88	0.26
ERA5-land	4.13	0.97	2.78	0.38
ERA5	4.11	0.98	2.77	0.36
GLDAS-Noah (0.25°)	4.14	0.87	2.90	0.37
MERRA2	4.10	0.88	2.90	0.32
JRA55	4.14	0.97	2.81	0.35
GLDAS-Noah (1°)	4.15	0.95	2.90	0.30
GLDAS-VIC (1°)	4.15	1.01	2.84	0.30
GLDAS-CLSM (1°)	4.15	1.06	2.79	0.30
Average	4.13	0.97	2.84	0.33
Percentage relative to total area	100%	23%	69%	8%

Text S5. Methods: Spatial and elevational integration

The pixel-scale quantities of swe_{peak}, s_{acc} and a_{acc} are further aggregated to the full HMA domain and at subregional scales, with persistent snow pixels (Text S4; Figure S2) masked out prior to the integration. Spatial integration of these quantities yields the same relationship as Equation (S3):

$$SWE_{peak} = S_{acc} - A_{acc} \tag{S5}$$

where SWE_{peak} is the pixel-wise peak SWE volume, and S_{acc} and A_{acc} respectively denote the cumulative snowfall and snow ablation volume integrated over the accumulation season. All three quantities are aggregated across the HMA-scale or subregional-scale domain.

Spatial integration over elevation bands is also detailed here (Figure S3). The DEM for each dataset (at the native resolution) is shown for a representative tile 34°N, 66°E in Figure S3a. The hypsometry over the whole domain (Figure S3b) shows how the areal distribution of elevation varies across datasets. For elevational distributions of variables (e.g. SWE_{peak} and S_{acc}), the native DEMs for each dataset were used to integrate into volumes by discretizing elevation bands using intervals of 1000 m (centered on 1500, 2500, 3500, 4500, and 5500 m). Compared with HMASR, all snow product DEMs have less area below 2000 m or above 3500 m, and more area in between (2000 – 3500 m). The hypsometry is generally consistent above 3500 m, and most different around 2500 m across snow products, with GLDAS (1°) showing the highest area, followed by JRA55 and MERRA2, while ERA5 and GLDAS (0.25°) show the least area (yet slightly higher than HMASR).

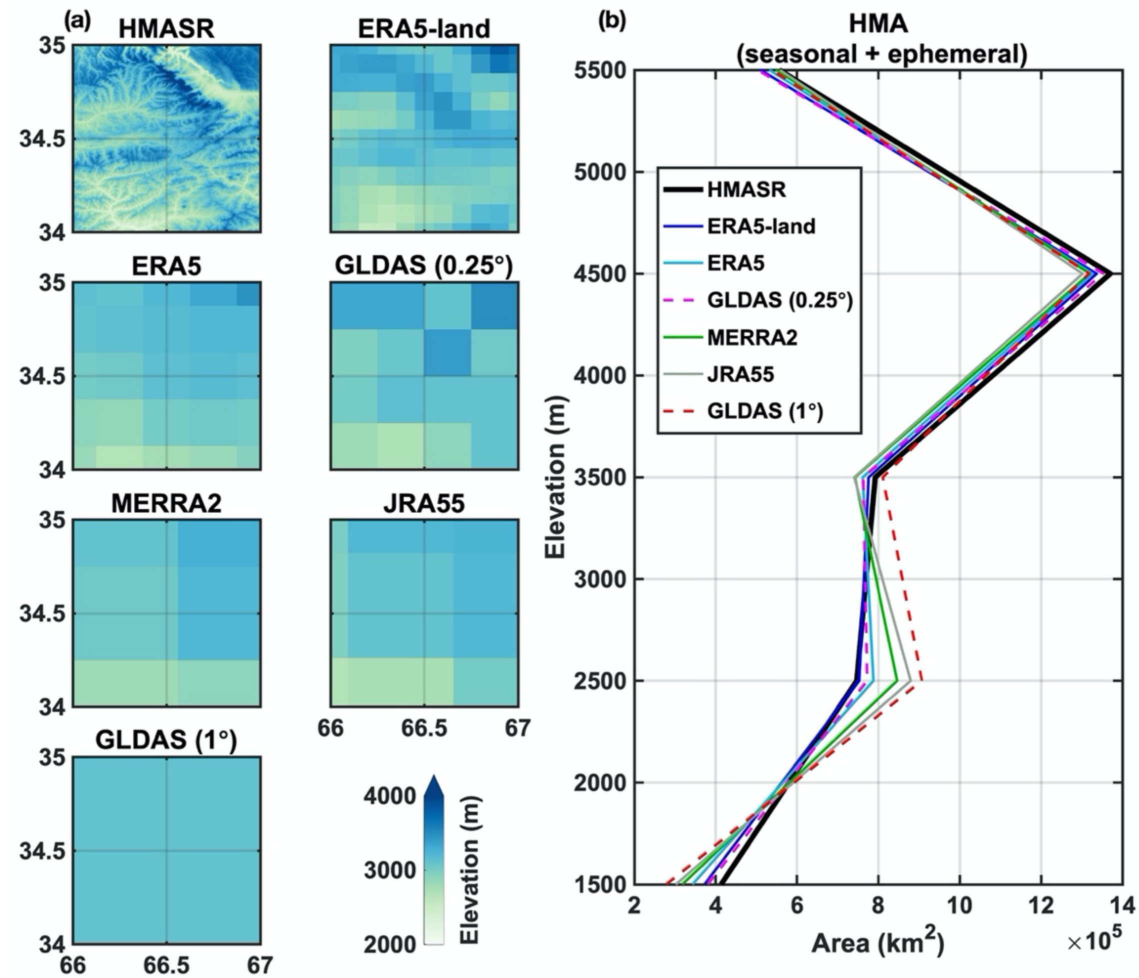

Figure S3. Illustration of dataset-specific **a**) DEMs for a representative tile (34°N, 66°E) at the native resolution and **b**) hypsometry over the HMA domain (masked with seasonal and ephemeral snow areas shown in Figure S1, with persistent snow and areas under 1500 m elevation excluded), integrated over 1000-m elevation bins (centered on 1500, 2500, 3500, 4500, and 5500 m).

Text S6: Methods: Linear regression

As shown in many previous studies, precipitation (in particular snowfall) is often regarded as the key variable affecting peak SWE estimation (Clark et al., 2011; Magnusson et al., 2015; Xu et al., 2019; Cho et al., 2022). Along these lines, we use a simple linear regression to examine the relationship between SWE_{peak} and S_{acc}:

$$SWE_{peak} = \beta * S_{acc} + \varepsilon \tag{S6}$$

where SWE_{peak} and S_{acc} are available for each snow product and each WY. In the analysis below, the regression is used to examine both global (i.e. across all snow products and WYs) and local (i.e. for a single snow product across all WYs) variations.

The β term is the regression coefficient (slope), and is derived either globally (β_{global}) or locally (β_i). The slope physically represents the fraction of cumulative snowfall that remains in the snowpack at t_{peak}. In the limit of no ablation the slope would be ~1, while the occurrence of accumulation-season ablation will generally lead to values < 1. The ε term is the random noise, which is assumed to be independent of the predictor (S_{acc}). To avoid collinearity, A_{acc} is not explicitly included as a predictor in the linear regression, as it is simply computed as the difference between S_{acc} and SWE_{peak} (Similar to Equation S4). The coefficient of determination (R^2) is often used to measure the goodness of fit for the linear model, and its value can be interpreted as the fraction of the explained variance. The above approach provides a mechanism to determine the relative role of snowfall vs. ablation in contributing to peak snow storage (through the slope) as well as explain the variation in peak storage relative to snowfall.

Text S7. Results: Climatology and uncertainty in HMA-wide peak snow storage

As referenced in the main text, Table S3 shows the 17-year climatology of SWE_{peak} in the eight global snow products, and their percent difference compared with those in HMASR.

Table S3. 17-year climatology of $\boldsymbol{SWE_{peak}}$ and the percent difference in the eight snow products compared to those in HMASR, over the full HMA domain and over the areas with seasonal and ephemeral snow.

	HMA		Seasonal		Ephemeral	
Dataset	$\boldsymbol{SWE_{peak}}$ (km^3)	% difference from HMASR	$\boldsymbol{SWE_{peak}}$ (km^3)	% difference from HMASR	$\boldsymbol{SWE_{peak}}$ (km^3)	% difference from HMASR
HMASR	239	-	210	-	30	-
ERA5-land	341	43%	249	19%	93	210%
ERA5	288	20%	198	-5%	90	200%
GLDAS-Noah (0.25°)	120	-50%	84	-60%	36	20%
MERRA2	54	-77%	35	-83%	18	-38%
JRA55	93	-61%	64	-69%	29	-3%
GLDAS-Noah (1°)	114	-53%	76	-64%	37	25%
GLDAS-VIC (1°)	179	-25%	113	-46%	65	119%
GLDAS-CLSM (1°)	98	-59%	61	-71%	38	26%
Mean (excluding HMASR)	161	-	110	-	51	-
Standard Deviation (excluding HMASR)	102	-	74	-	28	-
Mean Difference	-	-33%	-	-47%	-	70%
Root Mean Square Difference	-	52%	-	58%	-	113%

Text S8. Results: Elevational distribution in the volumetric fraction of S_{acc}, A_{acc} and SWE_{peak} climatology over the full HMA domain

The elevational distribution of S_{acc}, A_{acc} and SWE_{peak} climatology over the full HMA domain is shown in Figure S4, with volumes normalized by total S_{acc} to present the volumetric fraction. Given the significant differences in snowfall across snow products, the normalization reflects how, for the same amount of snowfall, each snow product distributes snowfall across elevation and how that fraction is partitioned into A_{acc} and SWE_{peak}. The elevational distribution over the full HMA domain exhibits a generally consistent pattern with that over the seasonal and ephemeral snow regimes. For convenience, we define the elevation bands centered on 2500 m, 3500 m and 4500 m as low-, mid- and high-elevation herein.

The fractional S_{acc} distribution over elevation is generally consistent across snow products, except that MERRA2 exhibits a slightly higher fraction at low-elevation and a lower fraction at high-elevation. ERA5 and ERA5-land exhibit higher S_{acc} fractions at mid-elevation (5% more than MERRA2) and lower fractions at high-elevation (comparable to MERRA2). The GLDAS products exhibits the lowest fractions at low-elevation (~ 5-8% less than MERRA2) but the highest fractions at high-elevation (~8% more than MERRA2).

The fractional A_{acc} distribution is significantly more distinct across snow products. At low- and mid-elevation, both ERA5-land and GLDAS-VIC stand out as having the lowest fractions, while ERA5 and the other GLDAS products show moderate fractions (8% more than ERA5-land), and MERRA2 shows the highest fraction (20% more than ERA5-land). At high-elevation, ERA5-land and GLDAS-VIC show the least fractional A_{acc}, but ERA5 exhibits a comparable fraction compared to ERA5-land. The other GLDAS products and MERRA2 show the highest fractions (8% more than ERA5-land). The extremely low ablation in ERA5-land and ERA5 at high-elevation is discussed in Hersbach et al. (2020) and is attributed to its single layer snow model not producing enough melt. The other three GLDAS products only exhibit minor difference with ~2% less fractional A_{acc} in GLDAS-Noah (0.25°) and 1% less fractional A_{acc} in GLDAS-Noah (1°) compared to GLDAS-CLSM at low-elevation, but barely exhibit any difference at mid- or high-elevation.

The elevational distribution of fractional SWE_{peak} is a direct result of fractional S_{acc} and A_{acc}. In general, ERA5-land exhibits the highest fractional SWE_{peak}, while MERRA2 has the lowest fraction, primarily because MERRA2 consistently has higher fractional A_{acc}. Their differences are the largest (13%) at mid-elevation where MERRA2 exhibits less fractional S_{acc}, and the smallest (5%) at low-elevation where MERRA2 exhibits more fractional S_{acc}. Compared with ERA5-land, GLDAS-VIC shows ~7% less fractional SWE_{peak} at mid-elevation, but ~6% more at high-elevation, primarily because of the difference in fractional S_{acc} distribution. Again, the other three GLDAS products exhibit a relatively consistent distribution in fractional SWE_{peak}, except for the 0.25° product, which shows a slightly higher fraction (~3%) at mid-elevation due to the fractional S_{acc} difference compared with other products. GLDAS also exhibits more fractional SWE_{peak} than MERRA2, with the largest difference (8%) at high-elevation where GLDAS obtains more fractional S_{acc} but equivalent fractional A_{acc}, and the smallest difference (<1%) at low-elevation where GLDAS exhibits less fractional S_{acc} and less fractional A_{acc}. These highlight the important role of ablation in removing snowfall differently with elevation, leading to a distinct distribution in fractional SWE_{peak} rather than just reproducing the fractional S_{acc} distribution.

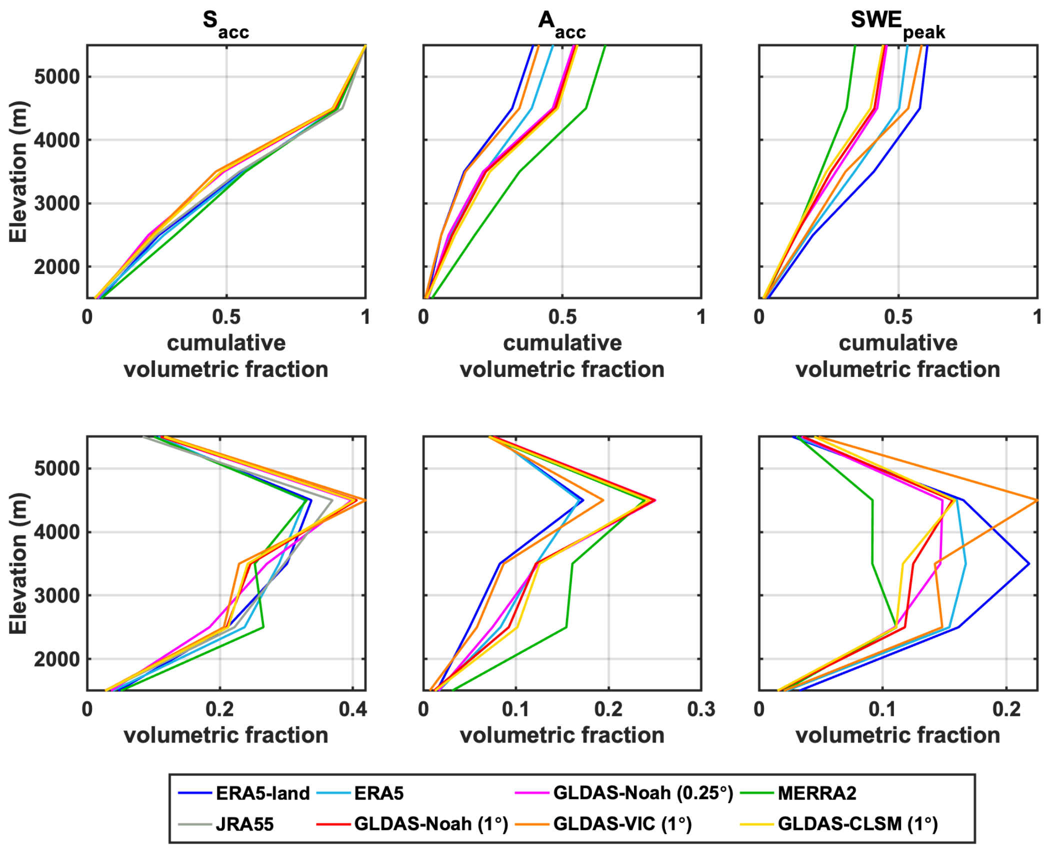

Figure S4. Volumetric fraction of accumulation-season snowfall ($\boldsymbol{S_{acc}}$), ablation ($\boldsymbol{A_{acc}}$) and peak SWE ($\boldsymbol{SWE_{peak}}$), integrated over 1000-m elevation bins (centered on 1500, 2500, 3500, 4500, and 5500 m) over the full HMA domain. The fractional distribution is obtained for each snow product by normalizing the distribution by the product-specific total $\boldsymbol{S_{acc}}$ across all elevations. The top panel displays the cumulative volumetric fraction across elevation bins, and the bottom panel displays the absolute volumetric fraction within elevation bins. Note that the fractional ablation and SWE in JRA55 are not displayed here, due to its diagnosed ablation being overestimated as a result of its snow data assimilation updates.

Text S9. Results: Explanations of peak snow storage variations from accumulation-season snowfall and ablation

As referenced in the main text, Table S4, Figure S5 and Figure S6 presented in this supplementary information are used to explain peak snow storage variations from accumulation-season snowfall and ablation.

Table S4 shows the linear regression statistics between SWE_{peak} and S_{acc} across WYs 2001-2017, with volumes integrated over the full HMA domain, seasonal and ephemeral snow regimes. As introduced in Text S6, regression is performed locally (for each snow product) and globally (across all snow product), with the exception of JRA55, which is not included in the global linear regression, due to its diagnosed ablation being overestimated as a result of its snow data assimilation updates.

Figure S5 shows the linear regression between SWE_{peak} and S_{acc} across WYs 2001-2017, with volumes integrated over the full HMA domain. The snow products are partitioned into two groups (subsets) (subset 1: GLDAS products and MERRA2, subset 2: ERA5 and ERA5-land), based on the notable gap between ERA5 and GLDAS seen from S_{acc}, where the linear statistics are obtained separately within each subset as shown on Figure S5.

Figure S6 shows the linear regression between S_{acc} and P_{acc} (accumulation-season precipitation) across WYs 2001-2017, with volumes integrated over the full HMA domain, to examine how much S_{acc} variations are explained by precipitation vs. rain-snow partitioning across snow products.

Table S4: Linear regression statistics of slope (β) and R^2, from global and local (snow product-specific regressions), where all regressions are statistically significant with p-values < 0.05. Note that JRA55 results are only displayed here (with statistics greyed-out in the table) but not included in the global linear regression due to its diagnosed ablation being overestimated as a result of its snow data assimilation updates.

	Slope ($\boldsymbol{\beta}$)			$\boldsymbol{R^2}$		
	HMA-wide	Seasonal	Ephemeral	HMA-wide	Seasonal	Ephemeral
Global	**0.54**	**0.71**	**0.35**	**0.88**	**0.88**	**0.80**
ERA5-land	0.61	0.83	0.35	0.58	0.94	0.25
ERA5	0.53	0.67	0.36	0.53	0.70	0.32
GLDAS-Noah (0.25°)	0.45	0.59	0.29	0.48	0.76	0.36
MERRA2	0.35	0.46	0.24	0.48	0.62	0.42
JRA55	0.25	0.30	0.17	0.61	0.77	0.33
GLDAS-Noah (1°)	0.45	0.58	0.29	0.46	0.76	0.35
GLDAS-VIC (1°)	0.58	0.76	0.41	0.60	0.83	0.48
GLDAS-CLSM (1°)	0.44	0.55	0.33	0.46	0.66	0.37

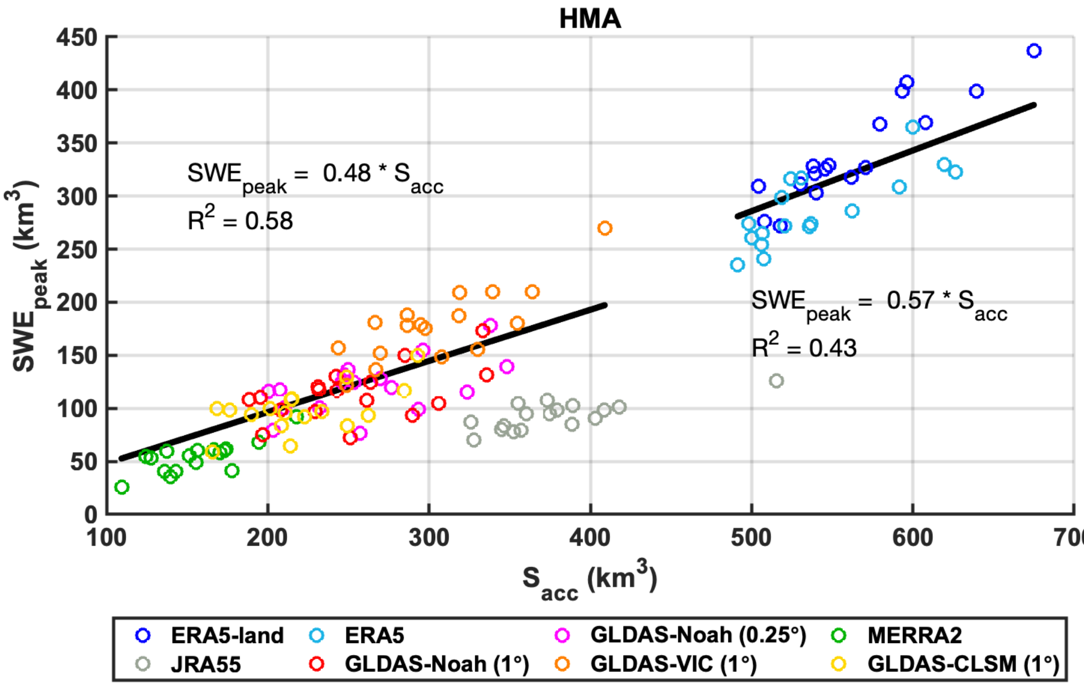

Figure S5. Regression of peak SWE volume (SWE_{peak}) and accumulation-season snowfall (S_{acc}) across WYs 2001-2017, with volumes integrated over the full HMA domain. Regression is performed over two subsets of datasets (subset 1: GLDAS products and MERRA2, subset 2: ERA5 and ERA5-land).

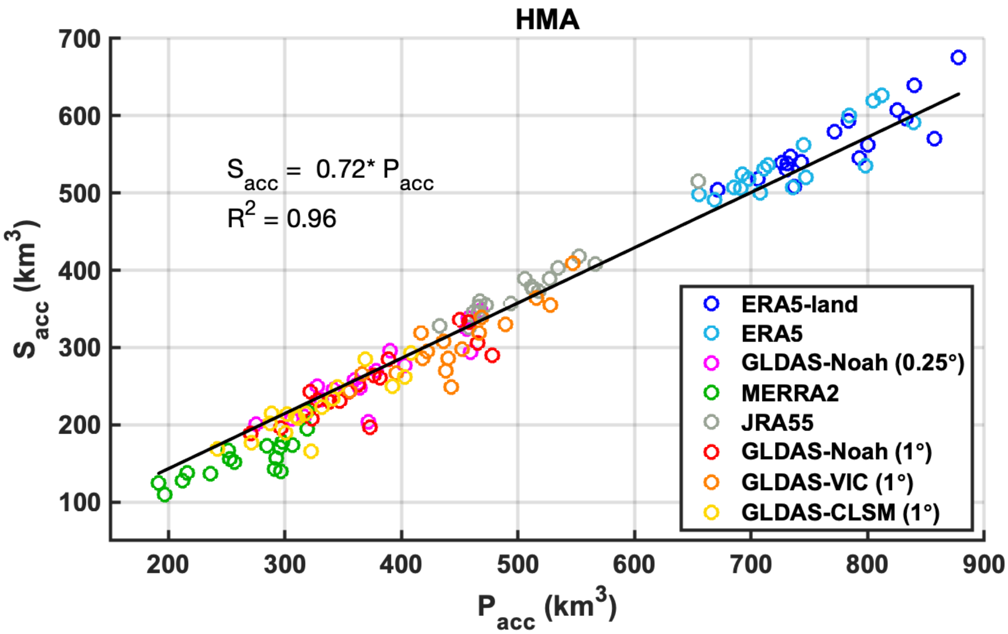

Figure S6. Regression of accumulation-season snowfall ($\boldsymbol{S_{acc}}$) vs. precipitation ($\boldsymbol{P_{acc}}$) across WYs 2001-2017, with volumes integrated over the full HMA domain.

SI references:

Bian, Q., Xu, Z., Zhao, L., Zhang, Y.-F., Zheng, H., Shi, C., Zhang, S., Xie, C., & Yang, Z.-L. (2019). Evaluation and Intercomparison of Multiple Snow Water Equivalent Products over the Tibetan Plateau. *Journal of Hydrometeorology*, *20*(10), 2043–2055. https://doi.org/10.1175/JHM-D-19-0011.1

Cho, E., Vuyovich, C. M., Kumar, S. V., Wrzesien, M. L., Kim, R. S., & Jacobs, J. M. (2022). Precipitation Biases and Snow Physics Limitations Drive the Uncertainties in Macroscale Modeled Snow Water Equivalent. *Hydrology and Earth System Sciences Discussions*, *2022*, 1–22. https://doi.org/10.5194/hess-2022-136

Clark, M. P., Hendrikx, J., Slater, A. G., Kavetski, D., Anderson, B., Cullen, N. J., Kerr, T., Örn Hreinsson, E., & Woods, R. A. (2011). Representing spatial variability of snow water equivalent in hydrologic and land-surface models: A review. *Water Resources Research*, *47*(7). https://doi.org/10.1029/2011WR010745

Gelaro, R., McCarty, W., Suárez, M. J., Todling, R., Molod, A., Takacs, L., Randles, C. A., Darmenov, A., Bosilovich, M. G., Reichle, R., Wargan, K., Coy, L., Cullather, R., Draper, C., Akella, S., Buchard, V., Conaty, A., da Silva, A. M., Gu, W., … Zhao, B. (2017). The Modern-Era Retrospective Analysis for Research and Applications, Version 2 (MERRA-2). *Journal of Climate*, *30*(14), 5419–5454. https://doi.org/10.1175/JCLI-D-16-0758.1

Hersbach, H., Bell, B., Berrisford, P., Hirahara, S., Horányi, A., Muñoz-Sabater, J., Nicolas, J., Peubey, C., Radu, R., Schepers, D., Simmons, A., Soci, C., Abdalla, S., Abellan, X., Balsamo, G., Bechtold, P., Biavati, G., Bidlot, J., Bonavita, M., … Thépaut, J.-N. (2020). The ERA5 global reanalysis. *Quarterly Journal of the Royal Meteorological Society*, *146*(730), 1999–2049. https://doi.org/10.1002/qj.3803

KOBAYASHI, S., OTA, Y., HARADA, Y., EBITA, A., MORIYA, M., ONODA, H., ONOGI, K., KAMAHORI, H., KOBAYASHI, C., ENDO, H., MIYAOKA, K., & TAKAHASHI, K. (2015). The JRA-55 Reanalysis: General Specifications and Basic Characteristics. *Journal of the Meteorological Society of Japan. Ser. II*, *93*(1), 5–48. https://doi.org/10.2151/jmsj.2015-001

Liu, Y., Fang, Y., & Margulis, S.A. (2021a). High Mountain Asia UCLA Daily Snow Reanalysis, Version 1. Boulder, Colorado USA, NASA Snow and Ice Data Center Distributed Active Archive Center. https://doi.org/10.5067/HNAUGJQXSCVU

Liu, Y., Fang, Y., & Margulis, S. A. (2021b). Spatiotemporal distribution of seasonal snow water equivalent in High Mountain Asia from an 18-year \hack\break Landsat–MODIS era snow reanalysis dataset. *The Cryosphere*, *15*(11), 5261–5280. https://doi.org/10.5194/tc-15-5261-2021

Magnusson, J., Wever, N., Essery, R., Helbig, N., Winstral, A., & Jonas, T. (2015). Evaluating snow models with varying process representations for hydrological applications. *Water Resources Research*, *51*(4), 2707–2723. https://doi.org/10.1002/2014WR016498

Muñoz-Sabater, J., Dutra, E., Agustí-Panareda, A., Albergel, C., Arduini, G., Balsamo, G., Boussetta, S., Choulga, M., Harrigan, S., Hersbach, H., Martens, B., Miralles, D. G., Piles, M., Rodríguez-Fernández, N. J., Zsoter, E., Buontempo, C., & Thépaut, J.-N. (2021). ERA5-Land: A state-of-the-art global reanalysis dataset for land applications. *Earth System Science Data*, *13*(9), 4349–4383. https://doi.org/10.5194/essd-13-4349-2021

ONOGI, K., TSUTSUI, J., KOIDE, H., SAKAMOTO, M., KOBAYASHI, S., HATSUSHIKA, H., MATSUMOTO, T., YAMAZAKI, N., KAMAHORI, H., TAKAHASHI, K., KADOKURA, S., WADA, K., KATO, K., OYAMA, R., OSE, T., MANNOJI, N., & TAIRA, R. (2007). The JRA-25 Reanalysis. *気象集誌. 第 2 輯*, *85*(3), 369–432. https://doi.org/10.2151/jmsj.85.369

Petersky, R., & Harpold, A. (2018). Now you see it, now you don't: A case study of ephemeral snowpacks and soil moisture response in the Great Basin, USA. *Hydrology and Earth System Sciences*, *22*(9), 4891–4906. https://doi.org/10.5194/hess-22-4891-2018

Reichle, R. H., Draper, C. S., Liu, Q., Girotto, M., Mahanama, S. P. P., Koster, R. D., & De Lannoy, G. J. M. (2017). Assessment of MERRA-2 Land Surface Hydrology Estimates. *Journal of Climate*, *30*(8), 2937–2960. https://doi.org/10.1175/JCLI-D-16-0720.1

Rodell, M., Houser, P. R., Jambor, U., Gottschalck, J., Mitchell, K., Meng, C.-J., Arsenault, K., Cosgrove, B., Radakovich, J., Bosilovich, M., Entin, J. K., Walker, J. P., Lohmann, D., & Toll, D. (2004). The Global Land Data Assimilation System. *Bulletin of the American Meteorological Society*, *85*(3), 381–394. https://doi.org/10.1175/BAMS-85-3-381

Sturm, M., Holmgren, J., & Liston, G. E. (1995). A Seasonal Snow Cover Classification System for Local to Global Applications. *Journal of Climate*, *8*(5), 1261–1283. https://doi.org/10.1175/1520-0442(1995)008<1261:ASSCCS>2.0.CO;2

Wrzesien, M. L., Pavelsky, T. M., Durand, M. T., Dozier, J., & Lundquist, J. D. (2019). Characterizing Biases in Mountain Snow Accumulation From Global Data Sets. *Water Resources Research*, *55*(11), 9873–9891. https://doi.org/10.1029/2019WR025350

Xu, Y., Jones, A., & Rhoades, A. (2019). A quantitative method to decompose SWE differences between regional climate models and reanalysis datasets. *Scientific Reports*, *9*(1), 16520. https://doi.org/10.1038/s41598-019-52880-5